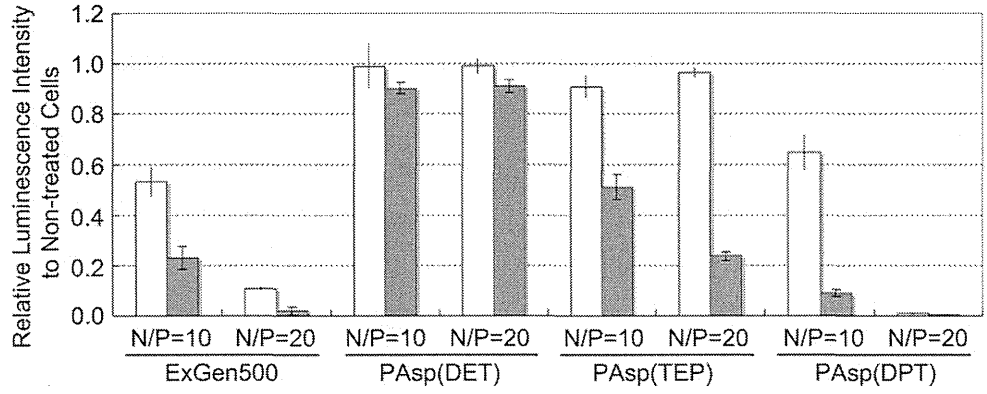

Fig. 5. Gene silencing efficiency of PICs evaluated by luciferase assay with B16F10-Luc cells. Scrambled siRNA (white bar) was adopted as a control sequence for luciferase siRNA (gray bar). Luciferase expression was measured after 48 h incubation with the PICs (siRNA: 100 nM). Results are expressed as the mean ± S.D. ($n = 4$).

3.4. Cellular uptake and intracellular distribution studies

To obtain an insight into the critical step in the transfection with the siRNA-loaded PICs tested here, the cellular uptake and intracellular distribution profiles were compared among the PICs. In the cellular uptake study, B16F10-Luc cells were treated by Cy3-siRNA-loaded PICs in the condition showing no severe cytotoxicity ($N/P = 10$ and 20 for PAsp(DET)/PAsp(TEP) and $N/P = 10$ for PAsp(DPT)) for 12 h, and then fluorescent signal from the cells was detected with a flow cytometer (Fig. 7). The cells treated by PAsp(TEP) and PAsp(DPT) PICs had one order of magnitude higher mean fluorescence intensity than those treated by PAsp(DET) PICs ($P < 0.01$), which showed the mean fluorescence comparable to the cells treated by naked Cy3-siRNA. This result indicated that the significant cellular uptake of PICs was achieved in the PAsp(DPT) and PAsp(TEP) system but not PAsp(DET) system. The obtained cellular uptake profiles were well correlated with the results of the stability (Fig. 4) and the gene silencing activity (Fig. 5) of the PICs, strongly suggesting that the stable PIC formation facilitated the cellular uptake of siRNA to exert effective gene silencing against the cultured cells. Interestingly, despite the similar PIC stability in the cell culture medium (Fig. 4), more efficient cellular uptake was observed for PAsp(DPT) PICs compared to PAsp(TEP) PICs ($P < 0.01$). The higher charge density in the side chain of PAsp(DPT) at pH 7.4 might facilitate the interaction of the PICs with the anionic components of cytoplasmic membrane leading to an increased efficiency of endocytosis [29]. Nevertheless, strong affinity of PAsp(DPT) with cytoplasmic membranes might impede the membrane integrity even at pH 7.4, causing a substantial increase in the cytotoxicity as seen in Fig. 6 [14].

Another critical step in siRNA delivery into the cytoplasm is endosomal escape [30]. The confocal laser scanning microscopic (CLSM) observation was performed to investigate the intracellular trafficking of Cy3-siRNA/PAsp(TEP) PIC at $N/P = 20$ and Cy3-siRNA/PAsp(DPT) PIC at $N/P = 10$, which achieved effective gene silencing without severe cytotoxicity (Figs. 5 and 6), by staining late endosome/lysosome and nucleus with LysoTracker Green (green) and Hoechst33342 (blue), respectively. Thus, in the CLSM images, the colocalization of Cy3-siRNA (red) with late endosome/lysosome (green) should be detected as yellow pixels. Fig. 8 clearly displayed the fluorescent signal from Cy3-siRNA (red and yellow pixels) within the cells treated by PAsp(TEP) and PAsp(DPT) PICs, consistent with the effective siRNA uptake as seen in the flow cytometric analysis (Fig. 7). To quantitatively estimate the endosomal escape of each PIC, the colocalization ratio of Cy3-siRNA with late endosome/lysosomes was determined from the ratio of the number of yellow pixels to the number of yellow/red pixels [22]. The colocalization ratios of Cy3-siRNA delivered by PICs were calculated to be ~26%

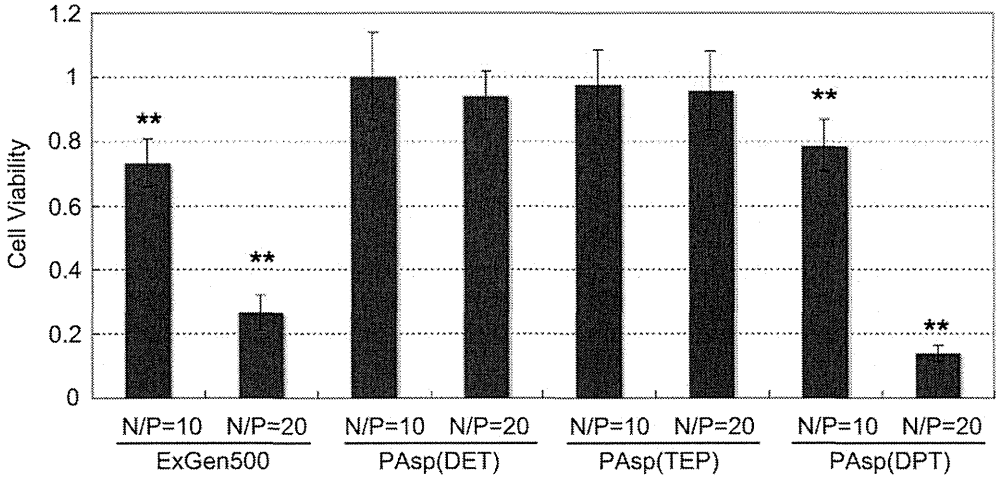

Fig. 6. Cytotoxicity of siRNA PICs against B16F10-Luc cells (siRNA: 100 nM) under the same condition as in the luciferase assay. Results are expressed as the mean ± S.D. ($n = 8$). ** indicates that the cells treated with each polyaspartamide derivative showed a significantly lower cell viability compared to the cells without any treatment ($P < 0.01$).

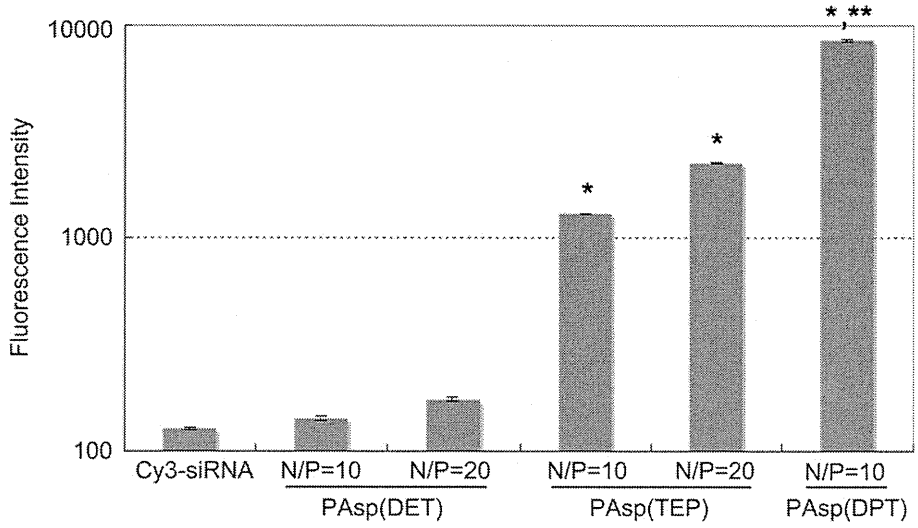

Fig. 7. Cellular uptake of siRNA PICs (siRNA: 100 nM) by B16F10-Luc cells after 12 h incubation measured with a flow cytometer. Results are expressed as the mean ± S.D. ($n = 3$). * indicates that cellular uptake of PICs was significantly higher than PAsp(DET) PIC and naked siRNA ($P < 0.01$). ** indicates that cellular uptake of PICs was significantly higher than PAsp(TEP) PICs prepared at N/P = 10 and 20 ($P < 0.01$).

for PAsp(TEP) at $N/P = 20$ and ~20% for PAsp(DPT) at $N/P = 10$, indicating that major portions of intracellular Cy3-siRNAs (~74% for PAsp(TEP) at $N/P = 20$ and ~80% for PAsp(DPT) at $N/P = 10$) were not distributed in late endosomal/lysosomal compartments 24 h after PIC administration, probably due to efficient endosomal escape. Note that the fluorescent signal of Cy3-siRNA from the cells treated by naked Cy3-siRNA or PAsp(DET) PICs was scarcely detected in this experimental condition (data not shown), corresponding to the poor siRNA uptake as seen in Fig. 7. Thus, we concluded that PAsp(TEP) and PAsp(DPT) appreciably improved both cellular uptake and endosomal escape of siRNA-loaded into their PICs.

3.5. Cellular membrane destabilization activity

From the results obtained in the preceding sections, PAsp(TEP) and PAsp(DPT) PICs were confirmed to facilitate cellular uptake and endosomal escape of loaded siRNA (Figs. 7 and 8), and consequently achieved the significant gene silencing (Fig. 5). However, the gene silencing of PAsp(DPT) PICs was accompanied by the cytotoxicity, which was in sharp contrast to PAsp(TEP) PICs showing comparable gene silencing without marked cytotoxicity (Fig. 6). Cytotoxicity of polycations is explained by the induction of impaired integrity of cytoplasmic membranes through their direct interaction with the anionic components of cytoplasmic membranes [11,14]; this mechanism may also play a role in an escape of polycation-based siRNA carriers from the acidic endosomal compartment. It should be noted that smart polycations increasing the capability to destabilize the membrane selectively in acidic milieu of endosome may lead to efficient but less toxic endosomal escape of their PICs [14].

Based on the fact that the side chain of PAsp(TEP) changed from the di-protonated state at pH 7.4 to tri-protonated state at pH 5.5 (Fig. 2), PAsp(TEP) is expected to have the acidic pH-selective membrane destabilization similar to PAsp(DET). We therefore evaluated the induction of the membrane destabilization by PAsp(TEP) in comparison with PAsp(DPT) and PAsp(DET) against B16F10-Luc cells at both extracellular pH of 7.4 and endosomal pH of 5.5. This study was evaluated by measuring the increased membrane permeability of YO-PRO-1 dye after incubating the cells with the polycations for 20 min (Fig. 9 and Fig. S1) [26]. Note that YO-PRO-1 is a cyanine dye staining DNA in the nucleus but it cannot permeate an intact cytoplasmic membrane of living cells. Therefore, the increased fluorescent signals of permeated YO-PRO-1 from living cell nuclei are expected to reflect the degree of membrane destabilization that would be induced by the polycations. As shown in Fig. 9, the cells treated with PAsp(TEP) exhibited negligible YO-PRO-1 fluorescence intensity at pH 7.4, while at pH 5.5 the PAsp(TEP) treatment induced a significant increase in the YO-PRO-1 fluorescence, indicating that PAsp(TEP) held the acidic pH-selective membrane destabilization capability in a similar manner as PAsp(DET). In contrast, PAsp(DPT) induced a significant increase in the YO-PRO-1 fluorescence corresponding to the strong membrane destabilization effect at both pH 7.4 and 5.5, which is consistent with its high cytotoxicity even under the physiological condition (Fig. 6).

In order to gain the insight into the mechanism of the membrane destabilization effect shown in Fig. 9, we focused on the types of polycations and their protonated structure varying with environmental pH. The significant increase in the YO-PRO-1 fluorescence compared to control was observed for PAsp(TEP) at pH 5.5, PAsp(DET) at pH 5.5, and PAsp(DPT) at pH 7.4 and 5.5 ($P < 0.01$), indicating the impaired membrane integrity In particular, the strongest effect was induced by PAsp(TEP) at pH 5.5. These trends suggest that the membrane destabilization effects might have some correlation with the number of protonated amines in the side chain of the polycations. Nevertheless, PAsp(TEP) at pH 7.4 displayed no significant membrane destabilization effect despite the side chain containing two protonated amines as PAsp(DPT). Of note is the spacer between two protonated amines in the side chain of each polycation (Fig. 2). The strong membrane destabilization was observed for the polycations with side chains having two protonated amines separated by the shorter spacers, i.e., ethylene spacer ($-CH_2CH_2-$) in PAsp(DET) and PAsp(TEP) at pH 5.5 and propylene spacer ($-CH_2CH_2CH_2-$) in PAsp(DPT) at pH 7.4 and 5.5. Alternatively, two protonated amines are separated by the longer spacer ($-CH_2CH_2NHCH_2CH_2-$ or $-CH_2CH_2NHCH_2CH_2NHCH_2CH_2-$) in PAsp(TEP) at pH 7.4. These results indicate that not only the number of cationic charges in the side chain but also their spacer length between protonated amines should be crucial to induce the membrane destabilization. The repeated protonated amines with shorter spacer length might enhance the capacity to perturb the

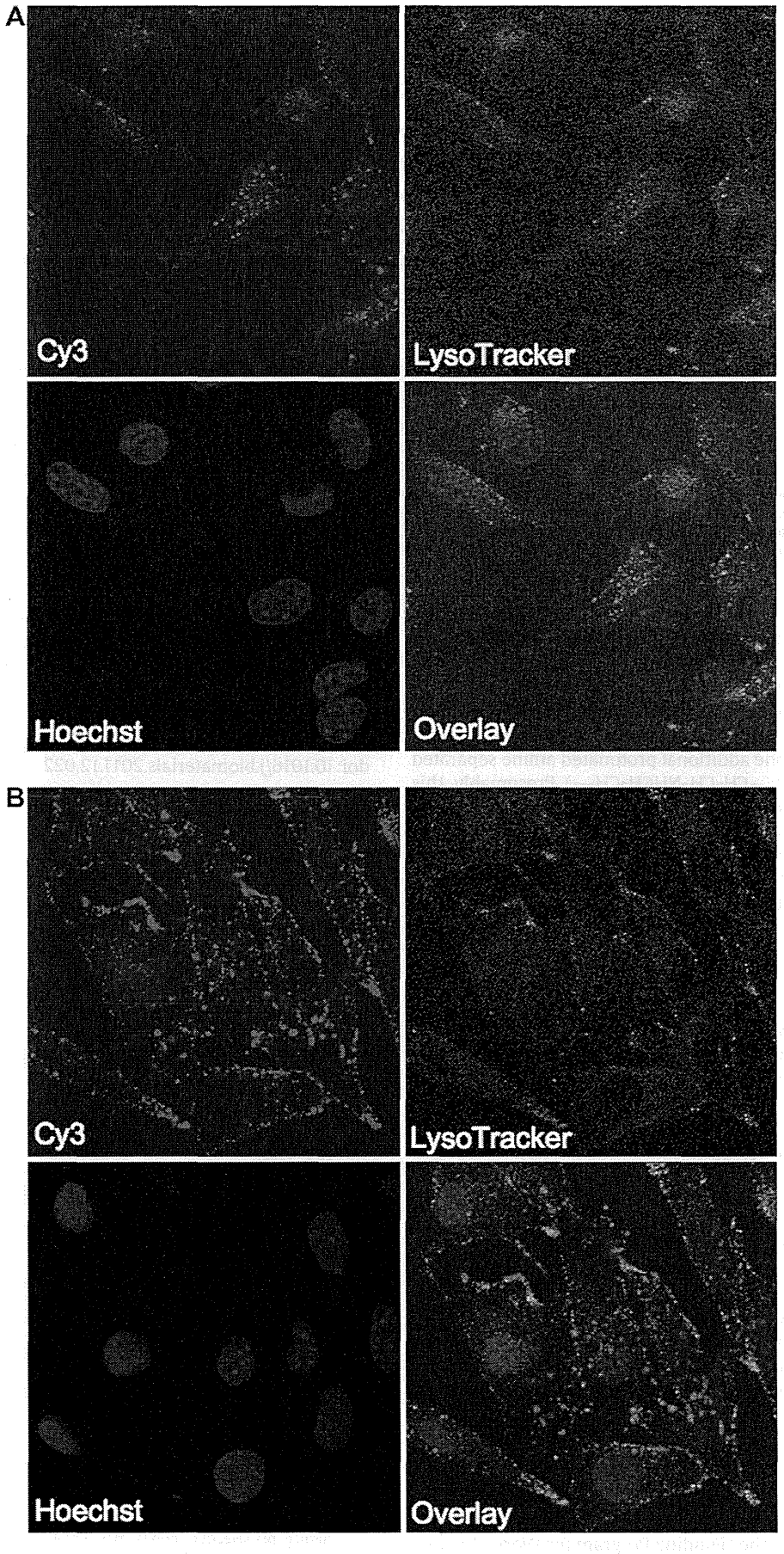

Fig. 8. Intracellular distribution of Cy3-siRNA PICs (siRNA: 100 nM) in B16F10-Luc cells after 24 h incubation, observed with confocal laser scanning microscope (Red: Cy3-siRNA, Green: *LysoTracker Green*, Blue: *Hoechst33342*). Each image represents the cells treated by PAsp(TEP) at $N/P = 20$ (A) and PAsp(DPT) at $N/P = 10$ (B). (For interpretation of the references to colour in this figure legend, the reader is referred to the web version of this article.)

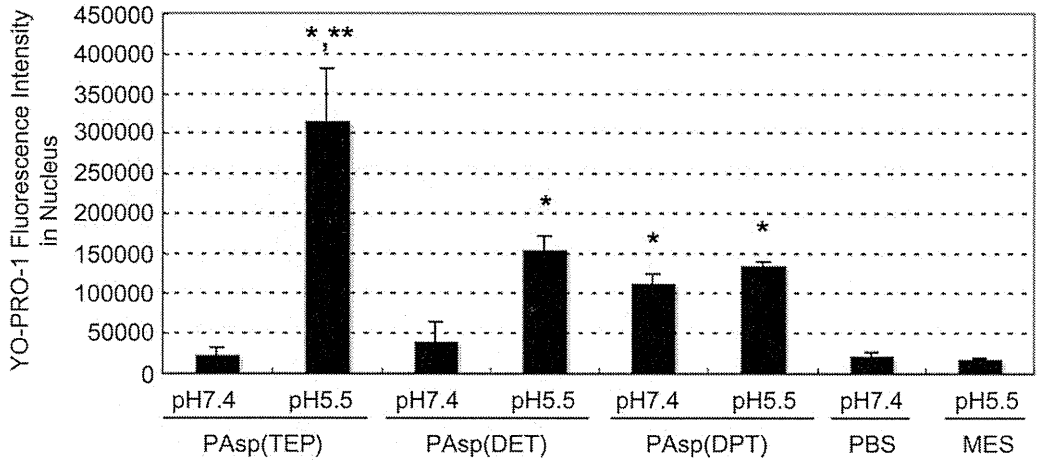

Fig. 9. Cellular membrane destabilization activity of each polyaspartamide derivative evaluated from the membrane permeability of YO-PRO-1 after incubation for 20 min with polyaspartamide derivatives, measured with In Cell Analyzer. The concentration of polycations was corresponding to that of PICs prepared at $N/P = 10$ in the luciferase assay. Results are expressed as the mean ± S.D. ($n = 3$). * indicates that the cells treated with each polyaspartamide derivative showed a significantly higher YO-PRO-1 fluorescence than cells treated with control (PBS for the treatment at pH 7.4 and MES for the treatment at pH 5.5) ($P < 0.01$), ** indicates that cells treated with PAsp(TEP) at pH 5.5 showed a significantly higher YO-PRO-1 fluorescence than cells treated with other polyaspartamide derivatives at pH 7.4 ($P < 0.01$) and pH 5.5 ($P < 0.05$).

membrane integrity through the facilitated binding of a multivalent array of cationic charges to the anionic component of cytoplasmic membrane. In line with this mechanism, PAsp(TEP) exerted appreciably high membrane disturbance effects at lowered pH of 5.5, where it took a tri-protonated state as a major component with two protonated amines linked by an ethylene spacer, fixing into *anti* conformation, and one additional protonated amine separated by flexible longer spacer ($-CH_2CH_2NHCH_2CH_2-$). Presumably, this characteristic arrayed structure of positive charges in PAsp(TEP) may lead to the unique and significant pH selectivity in YO-PRO-1 permeation through cytoplasmic membrane as seen in Fig. 9, thereby leading to effective endosomal escape and subsequent gene silencing with minimal cytotoxicity of siRNA/PAsp(TEP) PIC as demonstrated in Figs. 5, 6 and 8.

4. Conclusion

High stability both in storage condition and in biological milieu after the administration, effective cellular uptake with low cytotoxicity, and efficient endosomal escape leading to target-specific gene silencing are the major prerequisites for PIC-based siRNA carriers. The formation of stable siRNA-loaded PICs was demonstrated here from cationic polyaspartamide derivatives with a pH-valuable repeated array of protonated amines, exerting multivalent binding to siRNA molecules. Consequently, the constructed PIC achieved efficient cellular uptake due to enough tolerability in serum-containing medium and pH-selective disruption of cytoplasmic membranes for endosomal escape with minimal cytotoxicity and subsequent gene silencing with high efficiency. The number and the spacing length of repeating amino groups in the side chain of the polycations play a key role in these unique characteristics of the PIC, and the fine-tuning of these parameters is indispensable for translating PIC-based siRNA carriers into practical settings.

Acknowledgments

This research is granted by the Japan Society for the Promotion of Science (JSPS) through the "Funding Program for World-Leading Innovative R&D on Science and Technology (FIRST Program)," initiated by the Council for Science and Technology Policy (CSTP).

We express our appreciation to Dr. Darin Y. Furgeson (University of Utah) for proofreading of this manuscript.

Appendix. Supplementary material

Supplementary data related to this article can be found online at doi:10.1016/j.biomaterials.2011.12.022.

References

[1] Whitehead KA, Langer R, Anderson DG. Knocking down barriers: advances in siRNA delivery. Nat Rev Drug Discov 2009;8:129–38.
[2] Kabanov AV, Kabanov VA. DNA complexes with polycations for the delivery of genetic material into cells. Bioconjug Chem 1995;6:7–20.
[3] Kakizawa Y, Kataoka K. Block copolymer micelles for delivery of gene and related compounds. Adv Drug Deliv Rev 2002;54:203–22.
[4] Nishiyama N, Kataoka K. Current state, achievements, and future prospects of polymeric micelles as nanocarriers for drug and gene delivery. Pharm Ther 2006;112:630–48.
[5] Frohlich T, Wagner E. Peptide- and polymer-based delivery of therapeutic RNA. Soft Matter 2010;6:226–34.
[6] Boussif O, Lezoualc'h F, Zanta MA, Mergny MD, Scherman D, Demeneix B, et al. A versatile vector for gene and oligonucleotide transfer into cells in culture and in vivo: polyethylenimine. Proc Natl Acad Sci USA 1995;92:7297–301.
[7] Neu M, Fischer D, Kissel T. Recent advances in rational gene transfer vector design based on poly(ethylene imine) and its derivatives. J Gene Med 2005;7:992–1009.
[8] Schiffelers RM, Ansari A, Xu J, Zhou Q, Tang Q, Storm G, et al. Cancer siRNA therapy by tumor selective delivery with ligand-targeted sterically stabilized nanoparticle. Nucleic Acids Res 2004;32:e149.
[9] Ge Q, Filip L, Bai A, Nguyen T, Eisen HN, Chen J. Inhibition of influenza virus productin in virus-infected mice by RNA interference. Proc Natl Acad Sci USA 2004;101:8676–81.
[10] Alshamsan A, Haddadi A, Incani V, Samuel J, Lavasanifar A, Uludag H. Formulation and delivery of siRNA by oleic acid and stearic acid modified polyethylenimine. Mol Pharmaceutics 2009;6:121–33.
[11] Fischer D, Li Y, Ahlemeyer B, Krieglstein J, Kissel T. In vitro cytotoxicity testing of polycations: influence of polymer structure on cell viability and hemolysis. Biomaterials 2003;24:1121–31.
[12] Moghimi SM, Symonds P, Murray JC, Hunter AC, Debska G, Szewczyk A. A two-stage poly(ethylenimine)-mediated cytotoxicity: implications for gene transfer/therapy. Mol Ther 2005;11:990–5.
[13] Hunter AC. Molecular hurdles in polyfectin design and mechanistic background to polycation induced cytotoxicity. Adv Drug Deliv Rev 2006;58:1523–31.
[14] Miyata K, Oba M, Nakanishi M, Fukushima S, Yamasaki Y, Koyama H, et al. Polyplexes from poly(aspartamide) bearing 1,2-diaminoethane side chains induce pH-selective, endosomal membrane destabilization with amplified transfection and negligible cytotoxicity. J Am Chem Soc 2008;130:16287–94.
[15] Kanayama N, Fukushima S, Nishiyama N, Itaka K, Jang WD, Miyata K, et al. A PEG-based biocompatible block catiomer with high buffering capacity for

the construction of polyplex micelles showing efficient gene transfer toward primary cells. ChemMedChem 2006;1:439–44.
[16] Masago K, Itaka K, Nishiyama N, Chung UI, Kataoka K. Gene delivery with biocompatible cationic polymer: pharmacogenomic analysis on cell bioactivity. Biomaterials 2007;28:5169–75.
[17] Akagi D, Oba M, Koyama H, Nishiyama N, Miyata T, Nagawa H, et al. Biocompatible micellar nanovectors achieve efficient gene transfer to vascular lesions without cytotoxicity and thrombus formation. J Gene Med 2008;10. pp. 474–474.
[18] Itaka K, Ohba S, Miyata K, Kawaguchi H, Nakamura K, Takato T, et al. Bone regeneration by regulated in vivo gene transfer using biocompatible polyplex nanomicelles. Mol Ther 2007;15:1655–62.
[19] Harada-Shiba M, Takamisawa I, Miyata K, Ishii T, Nishiyama N, Itaka K, et al. Intratracheal gene transfer of adrenomedullin using polyplex nanomicelles attenuates monocrotaline-induced pulmonary hypertension in rats. Mol Ther 2009;17:1180–6.
[20] Oba M, Miyata K, Osada K, Christie RJ, Sanjoh M, Li W, et al. Polyplex micelles prepared from ω-cholesteryl PEG-polycation block copolymers for systemic gene delivery. Biomaterials 2011;32:652–63.
[21] Kim HJ, Ishii A, Miyata K, Lee Y, Wu S, Oba M, et al. Introduction of stearoyl moieties into a biocompatible cationic polyaspartamide derivative, PAsp(-DET), with endosomal escaping function for enhanced siRNA-mediated gene knockdown. J Control Release 2010;145:141–8.
[22] Takemoto H, Ishii A, Miyata K, Nakanishi M, Oba M, Ishii T, et al. siRNA-grafted polymer for polyion complex (PIC)-based siRNA delivery: enhancement of PIC stability and gene silencing efficiency. Biomaterials 2010;31:8097–105.
[23] Itaka K, Ishii T, Hasegawa Y, Kataoka K. Biodegradable polyamino acid-based polycations as safe and effective gene carrier minimizing cumulative toxicity. Biomaterials 2010;31:3707–14.
[24] Uchida H, Miyata K, Oba M, Ishii T, Suma T, Itaka K, et al. Odd-even effect of repeating aminoethylene units in the side chain of *N*-substituted polyaspartamides on gene transfection profiles. J Am Chem Soc 2011;133:15524–32.
[25] Harada A, Kataoka K. Formation of polyion complex micelles in an aqueous milieu from a pair of oppositely-charged block copolymers with poly(ethylene glycol) segments. Macromolecules 1995;28:5294–9.
[26] Uchida S, Itaka K, Chen Q, Osada K, Miyata K, Ishii T, et al. Combination of chondroitin sulfate and polyplex micelles of poly(ethylene glycol)-poly {N'-[N-(2-aminoethyl)-2-aminoethyl]aspartamide} block copolymer for prolonged in vivo gene transfection with reduced toxicity. J Control Release 2011;155:296–302.
[27] Nakanishi M, Park J-S, Jang W-D, Oba M, Kataoka K. Study of the quantitative aminolysis reaction of poly(β-benzyl L-aspartate) (PBLA) as a platform polymer for functionality materials. React Funct Polym 2007;67:1361–72.
[28] Buyens K, Meyer M, Wagner E, Demeester J, De Smedt SC, Sanders NN. Monitoring the disassembly of siRNA polyplexes in serum is crucial for predicting their biological efficacy. J Control Release 2010;141:38–41.
[29] Mislick KA, Baldeschwieler JD. Evidence for the role of proteoglycans in cation-mediated gene transfer. Proc Natl Acad Sci USA 1996;93:12349–54.
[30] Khalil IA, Kogure K, Akita H, Harashima H. Uptake pathways and subsequent intracellular trafficking in nonviral gene delivery. Pharmacol Rev 2006;58:32–45.

Efficient *In Vivo* Delivery of siRNA Into Brain Capillary Endothelial Cells Along With Endogenous Lipoprotein

Hiroya Kuwahara[1], Kazutaka Nishina[1], Kie Yoshida[1], Tomoko Nishina[1], Mariko Yamamoto[1], Yukari Saito[1], Wenying Piao[1], Masayuki Yoshida[2], Hidehiro Mizusawa[1] and Takanori Yokota[1]

[1]*Department of Neurology and Neurological Science, Graduate School, Tokyo Medical and Dental University, Tokyo, Japan;* [2]*Department of Life Science and Medical Ethics, Graduate School, Tokyo Medical and Dental University, Tokyo, Japan*

The brain capillary endothelial cell (BCEC) is a major functional component of the blood–brain barrier and is an underlying factor in the pathophysiology of various diseases, including brain ischemia, multiple sclerosis, and neurodegenerative disorders. We examined gene silencing in BCECs by using endogenous lipoprotein to introduce short-interfering RNA (siRNA) *in vivo*. A cholesterol-conjugated 21/23-mer siRNA targeting organic anion transporter 3 (*OAT3*) mRNA (Chol-siOAT3) was intravenously injected into mice after its incorporation into extracted endogenous lipoproteins. Chol-siOAT3 was not delivered to neurons or glia, but was successfully delivered into BCECs and resulted in a significant reduction of *OAT3* mRNA levels when injected after its incorporation into high-density lipoprotein (HDL). Efficient delivery was not achieved, however, when Chol-siOAT3 was injected without any lipoproteins, or after its incorporation into low-density lipoprotein (LDL). Investigations in apolipoprotein E (ApoE)-deficient and LDL receptor (LDLR)-deficient mice revealed that the uptake of HDL-containing Chol-siOAT3 was mainly mediated by ApoE and LDLR in mice. These findings indicate that siRNA can be delivered into BCECs *in vivo* by using endogenous lipoprotein, which could make this strategy useful as a new gene silencing therapy for diseases involving BCECs.

Received 3 February 2011; accepted 4 August 2011; advance online publication 13 September 2011. doi:10.1038/mt.2011.186

INTRODUCTION

The blood–brain barrier (BBB) is composed of brain capillary endothelial cells (BCECs) with pericytes, astrocyte foot processes, and nerve endings terminating on the capillary surface.[1] The BBB is a unique structure in the central nervous system that represents a physical barrier formed by endothelial tight junctions and a transport barrier resulting from selective membrane transporters and vesicular trafficking in the BCECs.[2]

BCECs are associated with the pathophysiology of various diseases, including brain ischemia, multiple sclerosis (MS), and neurodegenerative disorders.[3] *In vivo* gene silencing in BCECs can be a potentially useful approach for treating these above diseases because BCECs express different molecules that are considered to be important for the pathology of each disease. Inflammatory cell adhesion molecules, such as the intercellular adhesion molecule-1, vascular cell adhesion molecule-1, and selectins, are potential target molecules for the treatment of brain ischemia and MS. This is because the adhesion of activated leukocytes to BCECs induces secondary neuronal injury after reperfusion[4,5] and immune-mediated demyelination in MS.[6,7] In Alzheimer's disease (AD), inhibition of the receptor for advanced glycation end products (RAGE) can be expected to alleviate AD pathology, because RAGE expressed in BCECs mediates an influx transport of the neurotoxic amyloid-β peptide (Aβ) from the blood into the brain.[8,9]

RNA interference is a powerful tool to achieve post-transcriptional gene silencing. Efficient *in vivo* delivery of synthetic short-interfering RNA (siRNA) is the biggest challenge for the therapeutic application of this tool.[10] We first reported the delivery of siRNA into BCECs with a hydrodynamic injection technique,[11] and the same strategy was adopted in the subsequent reports.[12,13] However, the hydrodynamic injection technique cannot be applied clinically because of the volume overload and extremely high hydrostatic pressure involved; therefore, there is a need to develop an alternate strategy that would be clinically feasible.

We hypothesized that the best *in vivo* carrier of siRNA into BCECs is the molecule that is taken up into BCECs but cannot pass through the BBB. Cholesterol meets these requirements: cholesterol is a major lipid of lipoproteins which can be endocytosed via lipoprotein receptors expressed in BCECs, but most cholesterol cannot enter the brain.[14] Extracted endogenous lipoproteins have been reported to work as effective vectors for the delivery of siRNA to the liver by conjugation of cholesterol (Chol-siRNA).[15] This report showed that although Chol-siRNA incorporated into high-density lipoprotein (HDL) or low-density lipoprotein (LDL) accumulated in the liver, kidney, adrenal gland, ovary, stomach, and intestine, it was not detected in the brain after intravenous injection.[15] However, we suspect that it does not necessarily preclude the transport of Chol-siRNA into the BCECs, because the

Correspondence: *Takanori Yokota, Department of Neurology and Neurological Science, Graduate School, Tokyo Medical and Dental University, 1-5-45, Yushima, Bunkyo-ku, Tokyo 113-8519, Japan. E-mail: tak-yokota.nuro@tmd.ac.jp*

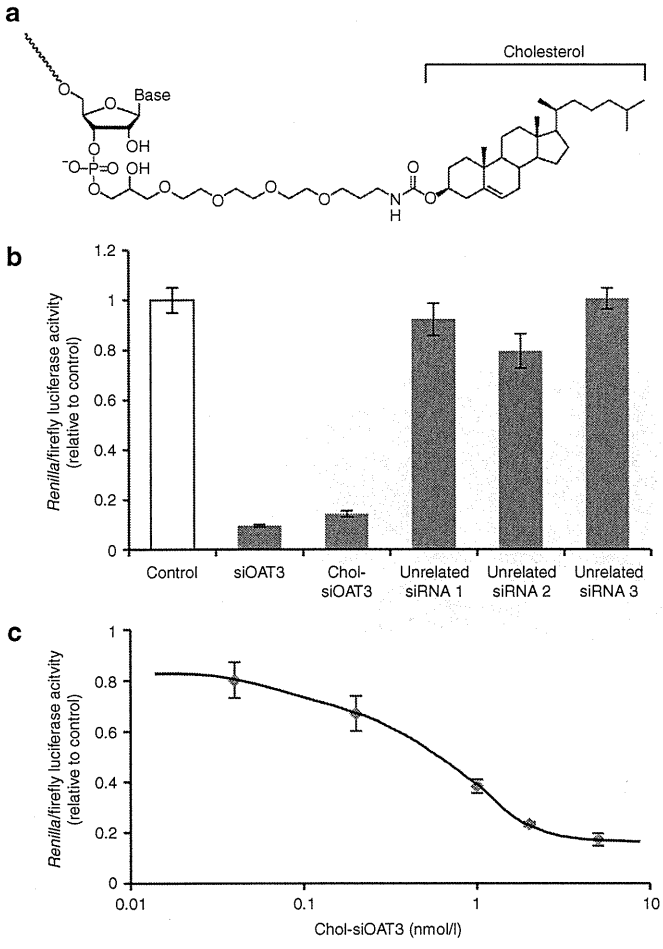

Figure 1 Design of Chol-siRNA targeting organic anion transporter 3 (*OAT3*) mRNA and its *in vitro* gene silencing effect. (**a**) Chemical structure of cholesterol conjugated to the 3′ end of the sense strand. (**b**) *In vitro* gene silencing effect of cholesterol-conjugated short-interfering RNA (siRNA) targeting *OAT3* mRNA (Chol-siOAT3). Luciferase activity was analyzed 24 hours after transfection of Neuro2a cells with the *Renilla* luciferase-fused *OAT3* expression vector, firefly luciferase expression vector, and either unconjugated siRNA targeting *OAT3* mRNA (siOAT3), Chol-siOAT3, or unrelated siRNA (unrelated siRNAs 1, 2, and 3 represent siRNAs targeting mouse claudin-5, apolipoprotein B, and superoxide dismutase-1, respectively) at the concentration of 5 nmol/l. The data shown are relative to the values of the control group (transfected without siRNA). Data are expressed as mean values ± SEM (n = 3). (**c**) *In vitro* gene silencing effect of Chol-siOAT3. Luciferase activity was analyzed 24 hours after transfection of Neuro2a cells with the *Renilla* luciferase-fused *OAT3* expression vector, firefly luciferase expression vector, and Chol-siOAT3 at different concentrations. Data are expressed as mean values ± SEM (n = 5). siRNA, short-interfering RNA; OAT3, organic anion transporter 3.

brain capillary endothelial volume is <0.1% of total brain[1] and therefore the distribution to the BCECs might be below the detection limit. In the present study, we have used endogenous lipoproteins to develop an *in vivo* delivery system for Chol-siRNA to be taken up into the BCECs.

RESULTS

Design of Chol-siRNA targeting *OAT3* mRNA and its *in vitro* gene silencing effect

We designed a 21/23-mer siRNA to target mouse *organic anion transporter 3* (*OAT3*) mRNA (NM_031194) so that there was an overhang of two nucleotides in the 3′-end of its antisense strand.[16] OAT3 is exclusively expressed at the endothelial cells in the brain and plays an important role in the brain-to-blood efflux transport of uremic toxins and neurotransmitter metabolites.[17] The siRNA sequence was taken from our previous report, which described the selection of a good sequence for the cleavage of *OAT3* mRNA.[11] Chemical modifications such as phosphorothioate linkages and 2′-*O*-methyl sugar modifications were introduced into the nucleotides at the 3′ side of the both strands of siRNA to enhance their resistance towards degradation by exo- and endonucleases.[18] Cholesterol was covalently conjugated to the 3′-end of the sense strand by using a cholesteryl-triethyleneglycol phosphoramidite linker (Chol-siOAT3) (Figure 1a).

Because the linker used to conjugate cholesterol was different from the pyrrolidine linker reported earlier,[18] we examined the *in vitro* gene silencing effect of Chol-siOAT3 by cotransfection of cultured mouse neuroblastoma (Neuro2a) cells with a *Renilla* luciferase-fused *OAT3* expression vector and a firefly luciferase expression vector. Chol-siOAT3 at the concentration of 5 nmol/l efficiently inhibited the expression of OAT3 by 86.6% relative to the control luciferase activity, an inhibition that was similar to that achieved by an unconjugated siRNA also targeting *OAT3* mRNA (siOAT3) (Figure 1b). The expression of OAT3 was not inhibited by unrelated siRNAs that targeted the mRNA of mouse claudin-5 (NM_013805), mouse apolipoprotein-B (*ApoB*) (NM_009693), or mouse superoxide dismutase-1 (NM_011434). The examination of the silencing effect of Chol-siOAT3 at different concentrations showed that the half maximal inhibitory concentration of Chol-siOAT3 was 0.51 nmol/l (Figure 1c). Thus, Chol-siOAT3 was considered to be highly efficient and specific in its cleavage of *OAT3* mRNA.

Ex vivo incorporation of Chol-siOAT3 into extracted endogenous lipoproteins

We investigated the character of endogenous lipoproteins used as vectors for Chol-siOAT3 and optimized the composition of *ex vivo* mixture of endogenous lipoproteins and Chol-siOAT3 for animal experiments. We first obtained endogenous lipoproteins from mouse sera by ultracentrifugation. The endogenous HDL fraction was isolated from the sera of wild-type (WT) mice, whereas the endogenous LDL fraction was collected from the sera of LDL receptor (LDLR)-deficient ($LDLR^{-/-}$) mice[19] because WT mice only had small amounts of LDL in their sera.

An analysis of lipid profiles using high-performance liquid chromatography[20] showed that the HDL fraction contained only HDL-cholesterol, with no cholesterol derived from any other lipoproteins (Figure 2a), and that the LDL fraction contained only LDL-cholesterol (Figure 2b). Moreover, western blotting revealed a characteristic apolipoprotein profile for each lipoprotein fraction: the HDL fraction contained apolipoprotein A-I (ApoA-I) and no ApoB, whereas the LDL fraction contained ApoB (ApoB-100 and ApoB-48) but no apolipoprotein A-I (Figure 2c). These results indicate that endogenous HDL and LDL had been successfully isolated.

Next, we incubated siOAT3 or Chol-siOAT3 with the HDL or LDL fraction *ex vivo* and evaluated the electrophoretic mobility of the resulting mixtures using polyacrylamide gels. Single bands

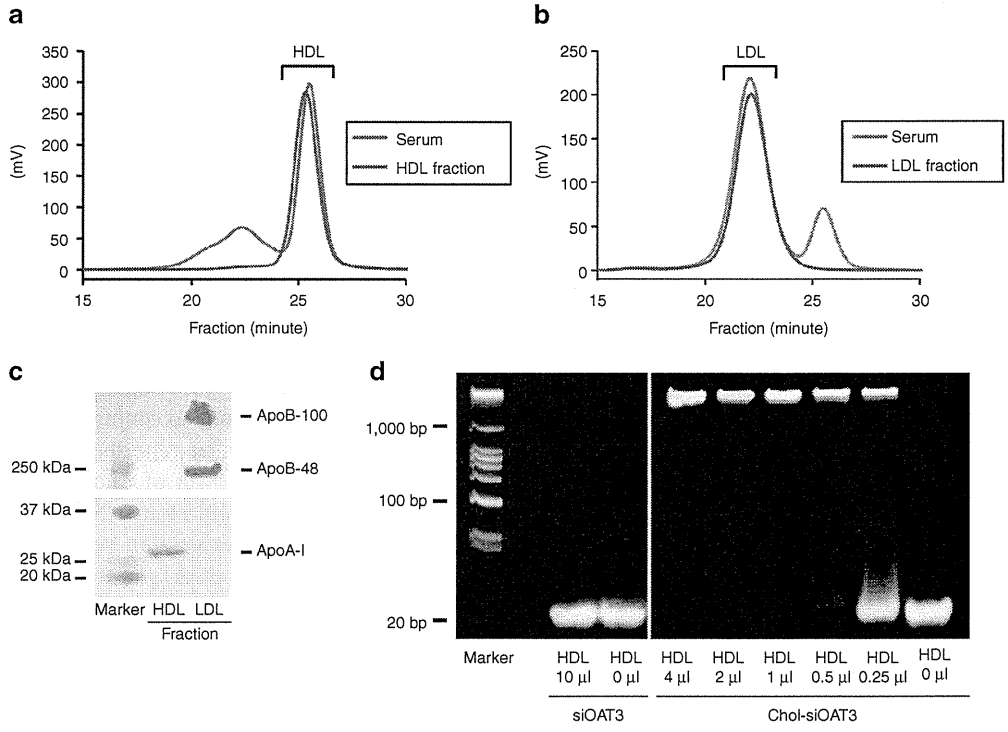

Figure 2 *Ex vivo* incorporation of Chol-siOAT3 into extracted endogenous lipoproteins. (**a**) HPLC analysis showing cholesterol levels of the serum and HDL fraction obtained from wild-type mice. (**b**) HPLC analysis showing cholesterol levels of the serum and LDL fraction obtained from LDL receptor-deficient (*LDLR*$^{-/-}$) mice. (**c**) Western blotting of ApoA-I and ApoB in the HDL and LDL fractions. (**d**) Gel-shift assay of siOAT3 and Chol-siOAT3. Electrophoretic mobility was examined using a 12% polyacrylamide gel after 100 pmol of each short-interfering RNA (siRNA) were incubated with different volumes of the HDL fraction. ApoA-I, apolipoprotein A-I; ApoB, apolipoprotein B; Chol-siOAT3, cholesterol-conjugated siRNA targeting *organic anion transporter 3* mRNA; HDL, high-density lipoprotein; HPLC, high-performance liquid chromatography; LDL, low-density lipoprotein; OAT3, organic anion transporter 3; siOAT3, unconjugated siRNA targeting *OAT3* mRNA.

were seen for siOAT3, both with and without the HDL fraction, at the position of ~21 nucleotides (Figure 2d). In contrast, mixtures of 100 pmol of Chol-siOAT3 and 1 µl and more of the HDL fraction did not show any bands corresponding to 21 nucleotides (Figure 2d). These mixtures were considered to be stable for at least 24 hours *in vivo* because the intensity and mobility of the mixtures did not change after the incubation with mouse sera at 37 °C for 24 hours (data not shown). Similar patterns of bands were seen when siOAT3 or Chol-siOAT3 was mixed with the LDL fraction (data not shown). Taken together, these results indicate that Chol-siOAT3 is incorporated into HDL and LDL in a saturable manner, whereas siOAT3 is not incorporated into these lipoproteins at all. We decided to mix 1 µl of the HDL or LDL fraction per 100 pmol of Chol-siOAT3 for animal experiments because Chol-siOAT3 could be fully incorporated into HDL or LDL at this ratio.

Delivery of Chol-siOAT3 into BCECs by intravenous injection

After siOAT3 and/or Chol-siOAT3 were injected into mice intravenously, we examined the extent of their delivery to the brain histologically. For this purpose, we utilized siRNAs labeled with Cy3 at the 5′-ends of the antisense strands. We injected 10 mg/kg of siOAT3 or Chol-siOAT3 alone [in phosphate-buffered saline (PBS)], or the same dosage of Chol-siOAT3 after its incorporation into HDL or LDL, into the tail vein. Brains of mice were taken 1 hour after the injection, and the frozen sections of the striatum were subjected to confocal laser imaging. We found no Cy3 signals in the brains after the injection of siOAT3 alone (Figure 3a). When mice were injected with Chol-siOAT3 without lipoproteins (Chol-siOAT3/PBS) or Chol-siOAT3 with the LDL fraction (Chol-siOAT3/LDL), there were faint Cy3 signals along the blood capillary vessels in the striatum (Figure 3a). In contrast, robust Cy3 signals were observed when mice were injected with Chol-siOAT3 with the HDL fraction (Chol-siOAT3/HDL) (Figure 3a). Similar findings were seen in all other areas of the brain, including the cerebral cortex, hippocampus, cerebellum, and the brainstem.

In mice injected with Chol-siOAT3/HDL, higher magnification of the brain sections revealed that Cy3 signals were located in the cytoplasm of BCECs that were marked immunologically by antibodies against von Willebrand factor (Figure 3b). There were no Cy3 signals in other cells of the brain, such as neurons or glia, indicating that Chol-siOAT3 could not pass through the BBB. Moreover, we found no Cy3 signals in the endothelial cells of the aorta and lung which were taken simultaneously at euthanization (data not shown).

For the detection of Chol-siOAT3 itself in the BCECs, we injected Chol-siOAT3 (10 mg/kg) with and without the lipoprotein fraction and performed northern blotting of small RNAs extracted from the small vascular fraction of the brain[21] 3 hours after injection with a probe corresponding to the antisense strand of Chol-siOAT3. The content of BCECs in the small vascular fraction of the brain was previously estimated to be ~50%[11] and thus,

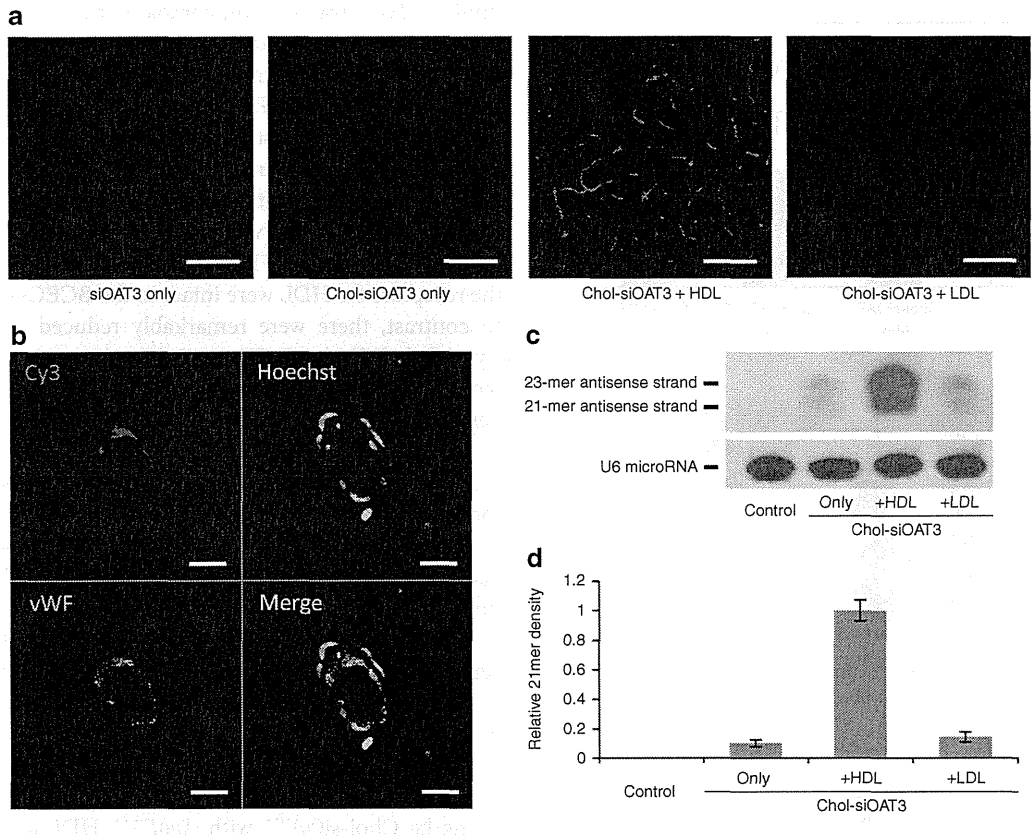

Figure 3 Delivery of Chol-siOAT3 into BCECs by intravenous injection. (**a**) Confocal laser images of frozen striatal sections prepared after intravenous injection of Cy3-labeled siOAT3 or Chol-siOAT3 (10 mg/kg), with and without the lipoprotein fraction. Bar = 100 μm. (**b**) Confocal laser images of frozen striatal sections prepared after intravenous injection of Cy3-labeled Chol-siOAT3 (10 mg/kg) along with HDL fraction. Sections were stained with Hoechst 33342 and immunolabeled with antibodies against vWF. Bar = 20 μm. (**c**) Northern blotting for the detection of antisense sequences of Chol-siOAT3 and the mouse U6 microRNA sequence in the small vascular fraction of the brain after injection of Chol-siOAT3 (10 mg/kg), with or without lipoprotein fractions. (**d**) The bars represent 21-mer band densities under the given conditions relative to band density of internal control, U6 microRNA. "Control" means uninjected; data are expressed as mean values ± SEM (n = 3). BCEC, brain capillary endothelial cell; Chol-siOAT3, cholesterol-conjugated short-interfering RNA targeting *organic anion transporter 3* mRNA; HDL, high-density lipoprotein; LDL, low-density lipoprotein; OAT3, organic anion transporter 3; siOAT3, unconjugated siRNA targeting *OAT3* mRNA; vWF, von Willebrand factor.

the detection of the antisense strand of Chol-siOAT3 by northern blotting was easier in this concentrated fraction than in the entire brain. The 21-mer band other than the 23-mer band was clearly detected when mice were injected with Chol-siOAT3/HDL (Figure 3c), suggesting that the 23-mer antisense strands had been cleaved by Dicer in the cytoplasm of BCECs. The density of the 21-mer band was much reduced when mice were injected with Chol-siOAT3/PBS or Chol-siOAT3/LDL (Figure 3c,d), demonstrating that the delivery of Chol-siOAT3 was only a little in these conditions. Taken together, these results indicate that Chol-siOAT3 is selectively delivered to the BCECs in the brain after intravenous injection and that the delivery is markedly enhanced when Chol-siOAT3 is incorporated into HDL before its injection into mice.

Gene silencing by intravenous injection of Chol-siOAT3 along with the HDL fraction

We assessed the extent of gene silencing after the intravenous injection of Chol-siOAT3. Mice were injected with 10 mg/kg Chol-siOAT3 with or without a lipoprotein fraction three times at 12-hour intervals, and were euthanized 6 hours after the last injection. Because OAT3 is exclusively expressed at endothelial cells in the brain, we could evaluate *OAT3* mRNA levels in BCECs by analyzing these levels in the entire brain. Quantitative reverse transcriptase-PCR (RT-PCR), which was performed using total RNA extracted from whole-brain homogenates, showed almost no reduction in *OAT3* mRNA levels when mice were injected with Chol-siOAT3/PBS or Chol-siOAT3/LDL (Figure 4a). In contrast, when mice were injected with Chol-siOAT3/HDL, *OAT3* mRNA levels in the brain were reduced by ~50% ($P < 0.01$; Figure 4a). We also evaluated *OAT3* mRNA levels in the kidneys of these mice because OAT3 was also expressed at the epithelial cells of the renal proximal tubules,[22] but there was no reduction (data not shown). The mRNA levels of interferon-β, interferon-γ, and tumor necrosis factor-α were not increased in the brains of these mice and there was no increase in the levels of interferon-α in the blood samples which were collected at euthanization from the mice injected with Chol-siOAT3/HDL, suggesting that there was no immune stimulatory effect contributing to the silencing activity (data not shown).

When mice were injected three times each with 1.0, 3.3, or 10 mg/kg of Chol-siOAT3 along with the HDL fraction (for total doses of 3, 10, and 30 mg/kg Chol-siOAT3), the 10 and 30 mg/kg total doses resulted in significant and dose-dependent reductions in *OAT3* mRNA levels (Figure 4b). We found no effects in

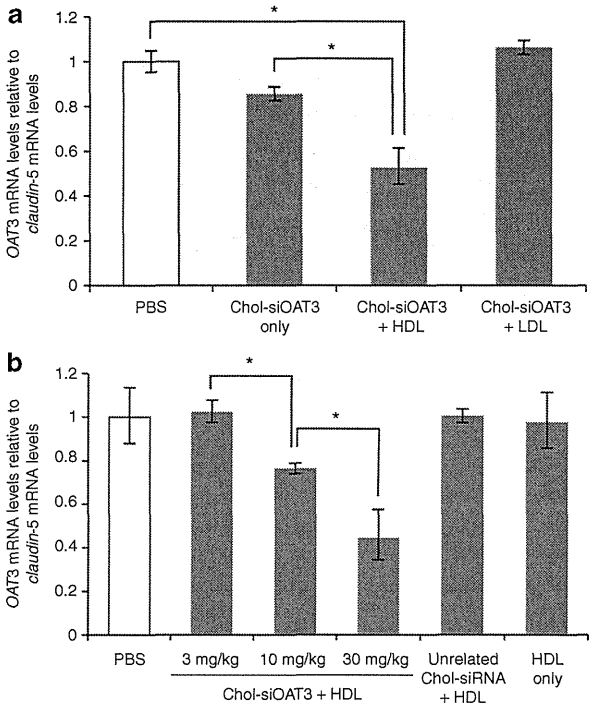

Figure 4 Gene silencing by intravenous injection of Chol-siOAT3 along with the HDL fraction. (**a**) Quantitative RT-PCR showing organic anion transporter 3 (*OAT3*) mRNA levels in whole-brain homogenates after the injection of Chol-siOAT3 (10 mg/kg), with and without lipoprotein fractions, three times at 12-hour intervals. The data shown are relative to claudin-5 mRNA levels and are expressed as mean values ± SEM ($n = 4$, $^*P < 0.01$). (**b**) Quantitative RT-PCR showing *OAT3* mRNA levels in whole-brain homogenates after the injection of different doses (1.0, 3.3, and 10 mg/kg) of Chol-siOAT3 with the HDL fraction, unrelated Chol-siRNA (10 mg/kg) with the HDL fraction, and HDL fraction only, three times at 12-hour intervals (Total injected dose is shown). The data shown are relative to claudin-5 mRNA levels and are expressed as mean values ± SEM ($n = 4$, $^*P < 0.01$). Chol-siOAT3, cholesterol-conjugated siRNA targeting *OAT3* mRNA; HDL, high-density lipoprotein; LDL, low-density lipoprotein; OAT3, organic anion transporter 3; PBS, phosphate-buffered saline; RT-PCR, reverse transcriptase-PCR.

the brain when mice were treated with an unrelated Chol-siRNA targeting *ApoB* mRNA (total dose 30 mg/kg) along with the HDL fraction, while there was a reduction of ~40% in the *ApoB* mRNA levels in the liver which was taken simultaneously at euthanization (data not shown). These results indicate that Chol-siOAT3 efficiently cleaves *OAT3* mRNA in BCECs when Chol-siOAT3 is incorporated into HDL before its injection into mice.

Receptor-mediated uptake of Chol-siOAT3/HDL into BCECs

We investigated the mechanism of delivery of Chol-siOAT3/HDL into BCECs. We thought that apolipoprotein E (ApoE) in HDL would most probably work as a ligand because of its important role in lipid transport.[23] First, we isolated endogenous HDL fractions from the sera of ApoE-deficient ($ApoE^{-/-}$ HDL)[24] and WT mice (WT HDL). To be able to make appropriate comparisons, we adjusted the mixed volume of each HDL fraction to have the same molecular amount of HDL-cholesterol. We then injected Cy3-labeled Chol-siOAT3 (10 mg/kg) into WT mice along with WT or $ApoE^{-/-}$ HDL fraction and compared the histological findings 1 hour later. The brain sections revealed similar Cy3 signals along the blood capillary vessels under both conditions (**Figure 5a**), suggesting that exogenous $ApoE^{-/-}$ HDL must recruit ApoE rapidly from the endogenous lipoproteins in the blood circulation of WT mice. Next, we injected the same dose of Cy3-labeled Chol-siOAT3 into $ApoE^{-/-}$ mice along with WT or $ApoE^{-/-}$ HDL fraction. Robust Cy3 signals were observed when Cy3-labeled Chol-siOAT3 was injected along with WT HDL fraction (**Figure 5b**), indicating that the receptors for HDL were intact in the BCECs of $ApoE^{-/-}$ mice. In contrast, there were remarkably reduced Cy3 signals when Cy3-labeled Chol-siOAT3 was injected into $ApoE^{-/-}$ mice along with $ApoE^{-/-}$ HDL fraction (**Figure 5b**), demonstrating that the delivery of Chol-siOAT3/HDL was mainly ApoE-dependent.

We tried further to identify the putative receptor for Chol-siOAT3/HDL in BCECs. Among several lipoprotein receptors expressed in BCECs, we hypothesized that LDLR was most likely to be responsible for the uptake of Chol-siOAT3/HDL because of its notably high affinity for ApoE.[23,25] The brain sections of $LDLR^{-/-}$ mice injected with Cy3-labeled Chol-siOAT3 along with WT HDL fraction revealed remarkably reduced Cy3 signals compared to the brain sections of WT mice injected with the same solution (**Figure 5c**), suggesting that Chol-siOAT3/HDL was taken up into BCECs mainly via LDLR.

Moreover, we assessed the gene silencing effect in the brains of $ApoE^{-/-}$ and $LDLR^{-/-}$ mice. $ApoE^{-/-}$ mice were injected with 10 mg/kg Chol-siOAT3 with $ApoE^{-/-}$ HDL and $LDLR^{-/-}$ mice were injected with 10 mg/kg Chol-siOAT3 with WT HDL three times at 12-hour intervals, and were euthanized 6 hours after the last injection. Quantitative RT-PCR showed no reduction in *OAT3* mRNA levels in the brains of $ApoE^{-/-}$ and $LDLR^{-/-}$ mice (**Figure 5d**). Taken together, these results indicate that the uptake of Chol-siOAT3/HDL into BCECs was mainly mediated by ApoE and LDLR in mice.

In vitro examinations of receptor-mediated uptake

We assessed *in vitro* whether LDLR could actually mediate the uptake of endogenous HDL. For this purpose, we utilized HEK293T cells transfected with a LDLR-expressing plasmid or a mock plasmid. The HDL fraction extracted from the sera of WT mice was mixed with a fluorescent lipid probe of BODIPY and was incubated in the culture medium of the HEK293T cells for 3 hours. LDLR-overexpressing cells showed marked BODIPY signals in the cytoplasm, whereas the cells transfected with mock plasmid showed almost no signals (**Figure 6a**), suggesting that extracted endogenous HDL could be taken up via LDLR.

Moreover, we evaluated *in vitro* whether the uptake of Chol-siOAT3/HDL into BCECs was mediated by scavenger receptor class B type I (SRBI) because SRBI was known as a major HDL receptor in the liver and was reported to be also expressed at BCECs.[26] For this purpose, we utilized the culture cells of conditionally immortalized brain capillary endothelium of mice origin, TM-BBB,[27] in which we confirmed the expression of *SRBI* mRNA by RT-PCR (data not shown). The cells were treated with a SRBI inhibitor, BLT-1,[28] and then incubated with 1 μmol/l of Cy3-labeled Chol-siOAT3/HDL for 30 minutes. Cy3 signals in the cytoplasm of TM-BBB cells were not decreased by BLT-1 (**Figure 6b**),

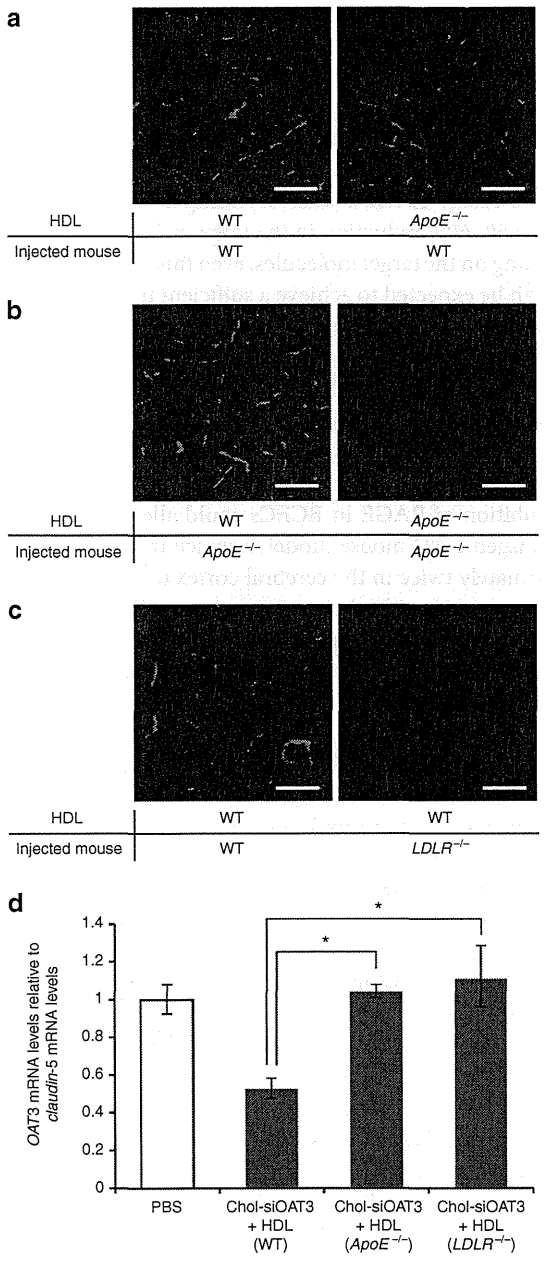

Figure 5 Receptor-mediated uptake of Chol-siOAT3/HDL into BCECs. (**a**) Confocal laser images of frozen striatal sections of WT mice after the injection of Cy3-labeled Chol-siOAT3 (10 mg/kg) with the HDL fraction extracted from the sera of WT or ApoE-deficient ($ApoE^{-/-}$) mice. Bar = 100 μm. (**b**) Confocal laser images of frozen striatal sections of $ApoE^{-/-}$ mice after the injection of Cy3-labeled Chol-siOAT3 (10 mg/kg) with the HDL fraction extracted from the sera of WT or $ApoE^{-/-}$ mice. Bar = 100 μm. (**c**) Confocal laser images of frozen striatal sections of WT and $LDLR^{-/-}$ mice after the injection of Cy3-labeled Chol-siOAT3 (10 mg/kg) with the HDL fraction extracted from the sera of WT mice. Bar = 100 μm. (**d**) Quantitative RT-PCR showing organic anion transporter 3 (*OAT3*) mRNA levels in whole-brain homogenates of WT, $ApoE^{-/-}$, and $LDLR^{-/-}$ mice after the injection of Chol-siOAT3 (10 mg/kg) with the HDL fraction, three times at 12-hour intervals. WT and $LDLR^{-/-}$ mice were injected with WT HDL, and $ApoE^{-/-}$ mice were injected with $ApoE^{-/-}$ HDL. The data shown are relative to claudin-5 mRNA levels and are expressed as mean values ± SEM ($n = 4$, $^*P < 0.01$). ApoE, apolipoprotein E; BCEC, brain capillary endothelial cell; Chol-siOAT3, cholesterol-conjugated siRNA targeting *OAT3* mRNA; HDL, high-density lipoprotein; LDLR, low-density lipoprotein receptor; OAT3, organic anion transporter 3; WT, wild-type.

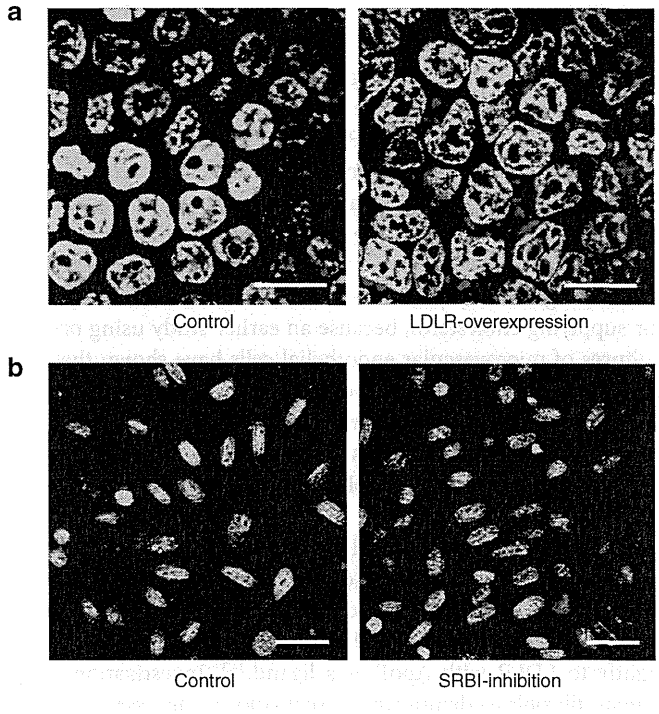

Figure 6 *In vitro* examinations of receptor-mediated uptake. (**a**) Confocal laser images of HEK293T cells transfected with a mock plasmid (Control) or a LDLR-expressing plasmid (LDLR-overexpression) 3 hours after incubation in the culture medium containing BODIPY-labeled HDL (red). Cells were stained with Hoechst 33342. Bar = 20 μm. (**b**) Confocal laser images of TM-BBB cells incubated with 1 μmol/l of Cy3-labeled Chol-siOAT3/HDL for 30 minutes with and without a pretreatment by 1 μmol/l of SRBI inhibitor. "Control" means no pretreatment by SRBI inhibitor. Cells were stained with Hoechst 33342. Bar = 20 μm. Chol-siOAT3, cholesterol-conjugated siRNA targeting *OAT3* mRNA; HDL, high-density lipoprotein; LDLR, low-density lipoprotein receptor; OAT3, organic anion transporter 3; SRBI, scavenger receptor class B type I.

suggesting that SR-BI was not a major receptor responsible for the uptake of Chol-siOAT3/HDL into BCECs.

DISCUSSION

In this study, we achieved efficient delivery of siRNA into BCECs by utilizing endogenous lipoproteins. We showed that Chol-siOAT3 was efficiently delivered into BCECs when incorporated into HDL before its intravenous injection, and that the mechanism of delivery was mainly receptor-mediated uptake.

When Chol-siOAT3 was injected without any lipoproteins, the delivery into BCECs was quite limited and resulted in very little gene silencing. Two explanations may account for this result. First, Chol-siOAT3 not incorporated into lipoproteins is rapidly removed from blood circulation through filtration in the kidneys and by uptake into the reticuloendothelial system such as the spleen, lymph nodes, and bone marrow.[10] Second, Chol-siOAT3 probably forms aggregates with other serum proteins, especially albumin,[15] resulting in its decreased incorporation into endogenous, circulating HDL. Chol-siOAT3 may attach itself to the plasma membrane of BCECs by virtue of its lipophilicity, but it is unlikely to be taken up by a nonspecific fluid-phase mechanism because there is minimal pinocytosis in BCECs.[1]

BCECs express lipoprotein receptors such as the LDLR, SRBI, and LDLR-related proteins.[2,26,29] The interaction of lipoproteins and BCECs has been investigated mostly from the perspective of lipoprotein transport to the brain across the BBB, rather than into the BCECs themselves. Plasma LDL can bind to LDLR in BCECs and pass through them via transcytosis to supply lipids to the brain.[29,30] Moreover, it has been suggested that plasma HDL can transport α-tocopherol to the brain by binding to SRBI and move via transcytosis across the BCECs.[26] Serum lipoproteins must also get transported into the BCECs themselves, especially for supplying cholesterol, because an earlier study using primary cultures of microvascular endothelial cells have shown that cholesterol synthesis in these cells decreases after addition of lipoproteins to the medium.[31] However, the precise mechanism of this transport—which lipoproteins are taken up into the BCECs and which receptors are responsible for this *in vivo* uptake—has not been elucidated.

Our results indicate that HDL works as an efficient vector for transporting Chol-siOAT3 into the BCECs, being mainly mediated by ApoE as the ligand and LDLR as the receptor. LDL binds to LDLR with ApoB-100 as a ligand, whereas HDL is also bound tightly to LDLR with ApoE as a ligand.[32,33] Investigations using human fibroblasts demonstrated that ApoE is necessary for HDL to not only bind to LDLR, but also to be internalized into the cells.[33] In the examinations using LDLR-overexpressing cells, we have also demonstrated that LDLR can mediate the uptake of endogenous HDL. On the other hand, SRBI was not considered to be a major receptor responsible for the uptake of Chol-siOAT3/HDL into BCECs because SRBI-inhibitor did not prevent the uptake of Chol-siOAT3/HDL into TM-BBB cells. SRBI is essentially responsible for the reverse cholesterol transport into hepatocytes and is mainly associated with the collection of cholesterol from the vascular endothelial cells into HDL, not the supply of cholesterol from HDL to these cells.[34] Therefore, we think it reasonable that the contribution of SRBI to the uptake of Chol-siOAT3/HDL into BCECs might be small. We suppose that in addition to LDLR, LDLR-related proteins can possibly mediate this uptake because LDLR-related proteins may be responsible for the supply of cholesterol into BCECs by virtue of its high affinity for ApoE.

Here we can ask why the delivery of Chol-siOAT3/LDL to BCECs via LDLR was not sufficiently achieved in WT mice, in spite of LDL uptake being the main function of LDLR. One possible explanation is the unique lipoprotein profile in rodents, which is different from those seen in other species. Because the rate of hepatic LDL clearance in rodents is 40 times greater than that in humans,[35] Chol-siOAT3/LDL may be getting rapidly eliminated from the blood circulation into the liver, resulting in limited distribution to other tissues or organs in mice. This explanation is consistent with the findings of an earlier study showing that Chol-siRNA was delivered almost exclusively to the mouse liver when it was incorporated into LDL, whereas with HDL, it was also distributed to the kidney, adrenal gland, ovary, stomach, and intestine.[15] Our negative result of *OAT3* mRNA suppression in the kidneys by Chol-siOAT3/HDL is probably and simply because the epithelial cells of the renal proximal tubules, in which OAT3 is expressed, are lined by the basement membrane and therefore do not directly face the blood circulation. As another explanation of the insufficient delivery of Chol-siOAT3/LDL to BCECs, we cannot rule out the possibility that LDL in $LDLR^{-/-}$ mice may have some unknown property that may be causing low affinity for LDLR. As a therapeutic approach in humans, LDL as well as HDL has a potential to work as another effective vector of Chol-siRNA to deliver the siRNA to BCECs in humans.

Our strategy of siRNA delivery using an HDL vector accomplished a 50–60% reduction in the target mRNA levels in BCECs. Depending on the target molecules, even this partial gene silencing effect can be expected to achieve a sufficient therapeutic outcome. A promising candidate gene for the treatment of AD is RAGE, which facilitates the transport of Aβ across the BBB into the brain[8] and therefore introduces the associated oxidative stress and neuroinflammation that characterize the disease.[9] The levels of RAGE are reported to be ~2.5-fold higher in the brains of AD patients than in age-matched controls.[8] Moreover, it is demonstrated that the inhibition of RAGE in BCECs could alleviate AD pathology in a transgenic AD mouse model in which the level of RAGE was approximately twice in the cerebral cortex of transgenic AD mice when compared with their nontransgenic littermate controls.[9] Thus, even a 50–60% reduction in the levels of RAGE in BCECs could be beneficial as a therapeutic intervention for AD patients.

The practicality of our strategy using endogenous lipoprotein should be also discussed. The volume of the HDL and LDL fraction in our experiments was half of mouse serum, and from a single series of ultracentrifugations, we obtained these fractions for 25 injections when mixed with 10 mg/kg of Chol-siRNA. We needed just one mouse for obtaining the HDL fraction for three injections with 10 mg/kg of Chol-siRNA, which accomplished a 50–60% reduction of target mRNA levels in BCECs. The dosing volume of 10 ml/kg body weight in our experiments is generally employed in the actual intravenous administration of blood products to patients, suggesting the feasibility of our strategy in the clinical situations.

Because lipoprotein vectors have been reported to accumulate mainly in the liver,[15] an enhancing their tropism toward BCECs would help to decrease the dose of Chol-siRNA and the lipoprotein vector. A recent study accomplished the delivery of increased amounts of a gene to BCECs by inserting polypeptides, selected from a phage library by *in vivo* panning, into the binding site of the adeno-associated virus vector to its receptor.[36] Similar approaches of engineering with polypeptides for Chol-siRNA and lipoprotein vectors should facilitate their enhanced targeting to BCECs and result in greater efficiency in gene silencing.

As another possible improvement of our strategy, recombinant lipoproteins can be better siRNA vectors because of their purity and homogeneity. Concerning the ApoE-based delivery, synthetic carriers including micelles and liposomes have been actually utilized for the delivery to BCECs *in vitro*.[37,38] However, it is not certain that recombinant lipoproteins can incorporate Chol-siRNA in the same manner as endogenous lipoprotein and that these artificial lipoproteins can be efficiently delivered to BCECs by the same receptor-mediated mechanism *in vivo*.

In summary, this is the first report to demonstrate the concept of an endogenous lipoprotein vector for the efficient delivery of siRNA into BCECs in mice via an intravenous injection. This concept of siRNA delivery can be advanced as a promising clinical

strategy for gene silencing to treat various diseases involving BCECs.

MATERIALS AND METHODS

siRNAs. All siRNAs were chemically synthesized at Hokkaido System Science (Sapporo, Japan). Cholesterol-conjugated siRNA targeting *OAT3* mRNA (Chol-siOAT3) was constituted from the corresponding sense strand: 5′-CCA UUA UCU UGA AUG UGG AAU*-cholesterol-3′ and antisense strand: 5′-AUU CCA CAU UCA AGA UAA UGg* u*G-3′. The lower case letters represent 2′-*O*-methyl sugar modification and the asterisks represent phosphorothioate linkages. Unconjugated siRNA targeting *OAT3* mRNA (siOAT3) was composed of the sense strand: 5′-CCA UUA UCU UGA AUG UGG AA*U-3′ and the same antisense strand as Chol-siOAT3. The unrelated siRNAs prepared for *in vitro* mRNA targeting were as follows: mouse claudin-5 (sense strand: 5′-CGU UGG AAA UUC UGG GUC UUU-3′, antisense strand: 5′-AGA CCC AGA AUU UCC AAC GUU-3′); mouse superoxide dismutase-1 (sense strand: 5′-GGU GGA AAU GAA GAA AGU ACA AAG ACU-3′, antisense strand: 5′-AGU CUU UGU ACU UUC UUC AUU UCC ACC UU-3′); and cholesterol-conjugated siRNA for *in vitro* and *in vivo* targeting of apolipoprotein-B mRNA (sense strand: 5′-GUC AUC ACA CUG AAU ACC AAU*-cholesterol-3′, antisense strand: 5′-AUU GGU AUU CAG UGU GAU GAc* a*C-3′).

Cholesterol was covalently conjugated via a cholesteryl-triethyleneglycol phosphoramidite linker (10-1975; Glen Research, Sterling, VA). For histological examinations, the 5′-ends of the antisense strands of siOAT3 and Chol-siOAT3 were labeled with Cy3. For the generation of siRNA duplexes, equimolar amounts of sense and antisense strands were heated in PBS at 95 °C for 5 minutes and slowly cooled to room temperature.

In vitro gene silencing. Mouse *OAT3* cDNA was subcloned from pGEM-HEN/Roct (OAT3) into the *Renilla* luciferase expression vector, psi-CHECK-1 (Promega, Fitchburg, WI). Neuro2a cells were transfected with 20 ng of a *Renilla* luciferase-fused *OAT3* expression vector, 50 ng of a firefly luciferase expression vector, pGL3 (Promega), and siRNA at different concentrations in each well of 24-well plates. Changes in *Renilla* luciferase activity were normalized to firefly luciferase activity. The luciferase activities were analyzed 24 hours after transfection by using the Dual Luciferase System (Promega).

Animals. Female WT imprinting control region mice (Oriental Yeast, Tokyo, Japan) were used to evaluate the extent of delivery of Chol-siOAT3 with and without lipoprotein fractions. Investigations of the mechanism of delivery of Chol-siOAT3/HDL were conducted in female $LDLR^{-/-}$ and $ApoE^{-/-}$ mice on a C57BL/6J background (The Jackson Laboratory, Bar Harbor, ME) and also with female WT C57BL/6J mice (Oriental Yeast). Mice were 8–10 weeks of age at the time of the studies and were kept on a 12-hour light/dark cycle in a pathogen-free animal facility with free access to food and water. All animal experiments were performed in accordance with the Ethical and Safety Guidelines for Animal Experiments of the Tokyo Medical and Dental University.

Isolation of lipoproteins. Lipoproteins were isolated from the sera of WT, $LDLR^{-/-}$, and $ApoE^{-/-}$ mice by ultracentrifugation, according to a modification of a method described earlier.[39] First, a half volume of a solution of density 1.006 g/ml was layered onto one volume of mouse serum and centrifuged for 2.4 hours at 337,000*g* at 16 °C. Second, one volume of the lower solution was mixed with a half volume of a solution of density 1.182 g/ml and centrifuged for 3.6 hours at 337,000*g* at 16 °C. The half volume of the upper solution was set aside for use in experiments as the LDL fraction, and one volume of the lower solution was mixed with a half volume of a solution of density 1.478 g/ml and centrifuged for 7.5 hours at 266,000*g* at 16 °C. The half volume of the upper solution obtained after this third centrifugation contained HDL and was used in experiments as the HDL fraction.

Western blotting analysis. Two microliters of HDL or LDL fraction were collected in 18 μl of homogenate buffer [20 mmol/l Tris–HCl (pH 7.4), 0.1% SDS, 0.1% Triton X-100, 0.01% sodium deoxycholate, and 1× complete protease inhibitor cocktail [Roche Diagnostics, Mannheim, Germany)]. The total protein mixture was separated by electrophoresis in a 5–20% polyacrylamide gel (ATTO, Tokyo, Japan) and transferred onto polyvinylidene difluoride membranes. Blots were probed with a goat antibody against ApoA-I (1:500, sc-23605; Santa Cruz Biotechnology, Santa Cruz, CA) and ApoB (1:500, sc-11795; Santa Cruz Biotechnology), and then incubated with an anti-goat secondary antibody (1:2,000, sc-2020; Santa Cruz Biotechnology) tagged with horseradish peroxidase. Blots were visualized with the aid of SuperSignal West Femto Maximum Sensitivity Substrate (Thermo Fisher Scientific, Waltham, MA) and analyzed with a ChemiDoc System (Bio-Rad, Hercules, CA).

Gel-shift assay. One hundred pmol of siOAT3 and Chol-siOAT3 were added to 0–10 μl of the HDL or LDL fraction. The samples were resolved by electrophoresis in a 12% polyacrylamide gel for 1 hour at 100 V. Two micrograms of siRNA ladder marker (Takara Bio, Otsu, Japan) was used as a size standard for siRNA. The siRNAs were visualized under ultraviolet light after staining the gel with ethidium bromide in Tris-borate-EDTA buffer.

Injection of siRNAs. Each siRNA was injected slowly into the tail veins of mice at a dosing volume of 10 ml/kg body weight in a single dose of 10 mg/kg for histological examinations and northern blotting analyses, and was injected three times in doses of 1.0, 3.3, or 10 mg/kg body weight at 12-hour intervals for quantitative RT-PCR.

Histological examination. Brains of mice were fixed in 4% paraformaldehyde/PBS for 12 hours. The fixed specimens were snap-frozen in liquid nitrogen and brain sections of 16-μm thickness were prepared by using a LEICA CM3050 S cryostat (Leica Microsystems, Wetzlar, Germany). The sections were stained with Hoechst 33342 (Sigma-Aldrich, St Louis, MO) to visualize the nuclei and were immunolabeled with antibodies against von Willebrand factor (1:100, A0082; Dako, Glostrup, Denmark) to visualize vascular endothelial cells. This was followed by incubation with a fluorescein isothiocyanate-conjugated secondary antibody (1:50, AP106F; Millipore, Billerica, MA). All images were acquired with an LSM 510 confocal laser scanning microscope (Carl Zeiss MicroImaging, Göttingen, Germany).

Small vascular fractionation of the brain and northern blotting analysis. The small vascular fraction of the brain was prepared according to a modification of a method reported earlier.[21] Briefly, brains of mice were homogenized in PBS and centrifuged for 5 minutes at 800*g*. The pellet was suspended in a 15% dextran solution and centrifuged for 10 minutes at 4,500*g* at 4 °C. The pellet was resuspended in 5 mmol/l PBS and, after incubation for 10 minutes, was centrifuged for 5 minutes at 800*g*. Small RNAs containing fewer than 200 nucleotides were extracted from the above final pellet of small vessels using MirVana (Ambion, Austin, TX). The RNA was condensed with Ethachinmate (Nippon Gene, Tokyo, Japan) and 1.2 μg of the RNA was separated by electrophoresis in a 14% polyacrylamide-urea gel and transferred to a Hybond-N^+ membrane (Amersham Biosciences, Piscataway, NJ). The blot was hybridized with a probe corresponding to the siRNA antisense sequence or with the mouse U6 microRNA sequence (as an internal control) which had been labeled with fluorescein using a Gene Images 3′-Oligolabelling Kit (Amersham Biosciences). The signals were visualized by Gene Images CDP-star Detection Kit (Amersham Biosciences).

Quantitative RT-PCR assay. Total RNA was extracted from whole-brain homogenates with Isogen (Nippon Gene). DNase-treated RNA (2.5 μg) was reverse-transcribed with Super Script III and Random Hexamers (Life Technologies, Carlsbad, CA). The cDNAs were amplified by

the quantitative TaqMan system by using the Light Cycler 480 Real-Time PCR Instrument (Roche Diagnostics). The primers and probes for mouse *OAT3* (Mm00459534_m1), claudin-5 (Mm00727012_s1), interferon-β (Mm00439546_s1), interferon-γ (Mm00801778_m1), and tumor necrosis factor-α (Mm00443258_m1) were designed by Life Technologies. Relative *OAT3* mRNA levels were calculated in comparison to claudin-5 mRNA levels, which were used as a BCEC-specific internal control.

Interferon-α analysis. The levels of interferon-α in the blood samples were analyzed by mouse interferon-α ELISA Kit (PBL Biomedical Laboratories, Piscataway, NJ) according to the manufacturers' protocol.

In vitro examinations of receptor-mediated uptake. Mouse serum HDL was labeled with BODIPY by a mixture of the HDL fraction and the solution of cholesteryl BODIPY 542/563 C11 (Life Technologies). HEK293T cells were grown in poly-D-lysine 4-well culture slides (BD, Franklin Lakes, NJ) and were transfected with 600 ng of mouse LDLR-expressing plasmid (Origene, Rockville, MD) or the same dose of mock plasmid by using Lipofectamine 2000 (Life Technologies). Twenty four hours after the transfection of the plasmids, the mixed solution containing 11 μl of the HDL fraction was added to 400 μl of the culture medium. After incubation for 3 hours, the cells were stained with Hoechst 33342 (Sigma-Aldrich) and were fixed in 4% paraformaldehyde/PBS.

TM-BBB cells (generously provided by Tetsuya Terasaki, PhD, Graduate School of Pharmaceutical Sciences, Tohoku University) were grown in collagen-I 4-well culture slides (BD) at 33 °C. The cells were treated with 1 μmol/l of SRBI inhibitor, BLT-1 (373210; Merck, Darmstadt, Germany) for 1 hour and then, were incubated with 1 μmol/l of Cy3-labeled Chol-siOAT3/HDL. After incubation for 30 minutes, the cells were stained with Hoechst 33342 (Sigma-Aldrich) and were fixed in 4% paraformaldehyde/PBS.

All images were acquired with an LSM 510 confocal laser scanning microscope (Carl Zeiss MicroImaging).

Statistical analysis. All data represent means ± SEM. Student's *t*-test was used to determine the significance of differences between two groups in quantitative RT-PCR assays.

ACKNOWLEDGMENTS

The authors thank Sumio Ohtsuki, PhD, Graduate School of Pharmaceutical Sciences, Tohoku University, for his helpful advice, and Mizuko Osaka, PhD, Department of Life Science and Medical Ethics, Graduate School, Tokyo Medical and Dental University, for her technical support. This work was supported by grants from the Ministry of Health, Labour, and Welfare of Japan (#2212070 and #2212148) and a grant from the Ministry of Education, Science and Culture of Japan (#20659138). This work was done in Tokyo, Japan. The authors declared no conflict of interest.

REFERENCES

1. Pardridge, WM (2007). Blood-brain barrier genomics. *Stroke* **38**(2 Suppl): 686–690.
2. Abbott, NJ, Patabendige, AA, Dolman, DE, Yusof, SR and Begley, DJ (2010). Structure and function of the blood-brain barrier. *Neurobiol Dis* **37**: 13–25.
3. Zlokovic, BV (2008). The blood-brain barrier in health and chronic neurodegenerative disorders. *Neuron* **57**: 178–201.
4. Frijns, CJ and Kappelle, LJ (2002). Inflammatory cell adhesion molecules in ischemic cerebrovascular disease. *Stroke* **33**: 2115–2122.
5. Danton, GH and Dietrich, WD (2003). Inflammatory mechanisms after ischemia and stroke. *J Neuropathol Exp Neurol* **62**: 127–136.
6. Correale, J and Villa, A (2007). The blood-brain-barrier in multiple sclerosis: functional roles and therapeutic targeting. *Autoimmunity* **40**: 148–160.
7. Simka, M (2009). Blood brain barrier compromise with endothelial inflammation may lead to autoimmune loss of myelin during multiple sclerosis. *Curr Neurovasc Res* **6**: 132–139.
8. Yan SD, Chen X, Fu J, Chen M, Zhu H, Roher A *et al.* (1996). RAGE and amyloid-beta peptide neurotoxicity in Alzheimer's disease. *Nature* **382**: 685–691.
9. Deane, R, Du Yan, S, Submamaryan, RK, LaRue, B, Jovanovic, S, Hogg, E *et al.* (2003). RAGE mediates amyloid-beta peptide transport across the blood-brain barrier and accumulation in brain. *Nat Med* **9**: 907–913.
10. Whitehead, KA, Langer, R and Anderson, DG (2009). Knocking down barriers: advances in siRNA delivery. *Nat Rev Drug Discov* **8**: 129–138.
11. Hino, T, Yokota, T, Ito, S, Nishina, K, Kang, YS, Mori, S *et al.* (2006). *In vivo* delivery of small interfering RNA targeting brain capillary endothelial cells. *Biochem Biophys Res Commun* **340**: 263–267.
12. Campbell, M, Kiang, AS, Kenna, PF, Kerskens, C, Blau, C, O'Dwyer, L *et al.* (2008). RNAi-mediated reversible opening of the blood-brain barrier. *J Gene Med* **10**: 930–947.
13. Fuest, C, Bankstahl, M, Winter, P, Helm, M, Pekcec, A and Potschka, H (2009). *In vivo* down-regulation of mouse brain capillary P-glycoprotein: a preliminary investigation. *Neurosci Lett* **464**: 47–51.
14. Pfrieger, FW (2003). Cholesterol homeostasis and function in neurons of the central nervous system. *Cell Mol Life Sci* **60**: 1158–1171.
15. Wolfrum, C, Shi, S, Jayaprakash, KN, Jayaraman, M, Wang, G, Pandey, RK *et al.* (2007). Mechanisms and optimization of *in vivo* delivery of lipophilic siRNAs. *Nat Biotechnol* **25**: 1149–1157.
16. Sano, M, Sierant, M, Miyagishi, M, Nakanishi, M, Takagi, Y and Sutou, S (2008). Effect of asymmetric terminal structures of short RNA duplexes on the RNA interference activity and strand selection. *Nucleic Acids Res* **36**: 5812–5821.
17. Ohtsuki, S, Asaba, H, Takanaga, H, Deguchi, T, Hosoya, K, Otagiri, M *et al.* (2002). Role of blood-brain barrier organic anion transporter 3 (OAT3) in the efflux of indoxyl sulfate, a uremic toxin: its involvement in neurotransmitter metabolite clearance from the brain. *J Neurochem* **83**: 57–66.
18. Soutschek, J, Akinc, A, Bramlage, B, Charisse, K, Constien, R, Donoghue, M *et al.* (2004). Therapeutic silencing of an endogenous gene by systemic administration of modified siRNAs. *Nature* **432**: 173–178.
19. Ishibashi, S, Brown, MS, Goldstein, JL, Gerard, RD, Hammer, RE and Herz, J (1993). Hypercholesterolemia in low density lipoprotein receptor knockout mice and its reversal by adenovirus-mediated gene delivery. *J Clin Invest* **92**: 883–893.
20. Usui, S, Hara, Y, Hosaki, S and Okazaki, M (2002). A new on-line dual enzymatic method for simultaneous quantification of cholesterol and triglycerides in lipoproteins by HPLC. *J Lipid Res* **43**: 805–814.
21. Kanda, T, Yoshino, H, Ariga, T, Yamawaki, M and Yu, RK (1994). Glycosphingolipid antigens in cultured bovine brain microvascular endothelial cells: sulfoglucuronosyl paragloboside as a target of monoclonal IgM in demyelinative neuropathy [corrected]. *J Cell Biol* **126**: 235–246.
22. Rizwan, AN and Burckhardt, G (2007). Organic anion transporters of the SLC22 family: biopharmaceutical, physiological, and pathological roles. *Pharm Res* **24**: 450–470.
23. Mahley, RW (1988). Apolipoprotein E: cholesterol transport protein with expanding role in cell biology. *Science* **240**: 622–630.
24. Zhang, SH, Reddick, RL, Piedrahita, JA and Maeda, N (1992). Spontaneous hypercholesterolemia and arterial lesions in mice lacking apolipoprotein E. *Science* **258**: 468–471.
25. Hatters, DM, Peters-Libeu, CA and Weisgraber, KH (2006). Apolipoprotein E structure: insights into function. *Trends Biochem Sci* **31**: 445–454.
26. Balazs, Z, Panzenboeck, U, Hammer, A, Sovic, A, Quehenberger, O, Malle, E *et al.* (2004). Uptake and transport of high-density lipoprotein (HDL) and HDL-associated alpha-tocopherol by an *in vitro* blood-brain barrier model. *J Neurochem* **89**: 939–950.
27. Hosoya, K, Tetsuka, K, Nagase, K, Tomi, M, Saeki, S, Ohtsuki, S *et al.* (2000). Conditionally immortalized brain capillary endothelial cell lines established from a transgenic mouse harboring temperature-sensitive simian virus 40 large T-antigen gene. *AAPS PharmSci* **2**: E27.
28. Nieland, TJ, Shaw, JT, Jaipuri, FA, Duffner, JL, Koehler, AN, Banakos, S *et al.* (2008). Identification of the molecular target of small molecule inhibitors of HDL receptor SR-BI activity. *Biochemistry* **47**: 460–472.
29. Goti, D, Balazs, Z, Panzenboeck, U, Hrzenjak, A, Reicher, H, Wagner, E *et al.* (2002). Effects of lipoprotein lipase on uptake and transcytosis of low density lipoprotein (LDL) and LDL-associated alpha-tocopherol in a porcine *in vitro* blood-brain barrier model. *J Biol Chem* **277**: 28537–28544.
30. Dehouck, B, Fenart, L, Dehouck, MP, Pierce, A, Torpier, G and Cecchelli, R (1997). A new function for the LDL receptor: transcytosis of LDL across the blood-brain barrier. *J Cell Biol* **138**: 877–889.
31. Roux, FS, Mokni, R, Hughes, CC, Clouet, PM, Lefauconnier, JM and Bourre, JM (1989). Lipid synthesis by rat brain microvessel endothelial cells in tissue culture. *J Neuropathol Exp Neurol* **48**: 437–447.
32. Jeon, H and Blacklow, SC (2005). Structure and physiologic function of the low-density lipoprotein receptor. *Annu Rev Biochem* **74**: 535–562.
33. Mahley, RW and Innerarity, TL (1977). Interaction of canine and swine lipoproteins with the low density lipoprotein receptor of fibroblasts as correlated with heparin/manganese precipitability. *J Biol Chem* **252**: 3980–3986.
34. Connelly, MA and Williams, DL (2004). Scavenger receptor BI: a scavenger receptor with a mission to transport high density lipoprotein lipids. *Curr Opin Lipidol* **15**: 287–295.
35. Dietschy, JM and Turley, SD (2002). Control of cholesterol turnover in the mouse. *J Biol Chem* **277**: 3801–3804.
36. Chen, YH, Chang, M and Davidson, BL (2009). Molecular signatures of disease brain endothelia provide new sites for CNS-directed enzyme therapy. *Nat Med* **15**: 1215–1218.
37. Sauer, I, Dunay, IR, Weisgraber, K, Bienert, M and Dathe, M (2005). An apolipoprotein E-derived peptide mediates uptake of sterically stabilized liposomes into brain capillary endothelial cells. *Biochemistry* **44**: 2021–2029.
38. Leupold, E, Nikolenko, H and Dathe, M (2009). Apolipoprotein E peptide-modified colloidal carriers: the design determines the mechanism of uptake in vascular endothelial cells. *Biochim Biophys Acta* **1788**: 442–449.
39. Hatch, FT (1968). Practical methods for plasma lipoprotein analysis. *Adv Lipid Res* **6**: 1–68.

Biomacromolecules

ARTICLE

pubs.acs.org/Biomac

Effect of Polymer Structure on Micelles Formed between siRNA and Cationic Block Copolymer Comprising Thiols and Amidines

R. James Christie,[†] Kanjiro Miyata,[‡,§,∥] Yu Matsumoto,[‡,⊥,#] Takahiro Nomoto,[∥] Daniel Menasco,[○] Tzai Chung Lai,[○] Matthew Pennisi,[†] Kensuke Osada,[†,§] Shigeto Fukushima,[†] Nobuhiro Nishiyama,[‡] Yuichi Yamasaki,[†,§] and Kazunori Kataoka*[,†,‡,§,∥]

[†]Department of Materials Engineering, Graduate School of Engineering, The University of Tokyo, Japan

[‡]Division of Clinical Biotechnology, Center for Disease Biology and Integrative Medicine, Graduate School of Medicine, The University of Tokyo, Japan

[§]Center for NanoBio Integration, The University of Tokyo, Japan

[∥]Department of Bioengineering, Graduate School of Engineering, The University of Tokyo, Japan

[⊥]Department of Otorhinolaryngology and Head and Neck Surgery, Graduate School of Medicine and Faculty of Medicine, The University of Tokyo, Japan

[#]Department of Otorhinolaryngology and Head and Neck Surgery, Mitsui Memorial Hospital, Japan

[○]Center for Medical Systems Innovation Summer Internship Program, The University of Tokyo, Japan

Supporting Information

ABSTRACT: Small interfering RNA (siRNA) has great therapeutic potential for the suppression of proteins associated with disease, but delivery methods are needed for improved efficacy. Here, we investigated the properties of micellar siRNA delivery vehicles prepared with poly(ethylene glycol)-*block*-poly(L-lysine) (PEG-*b*-PLL) comprising lysine amines modified to contain amidine and thiol functionality. Lysine modification was achieved using 2-iminothiolane (2-IT) [yielding PEG-*b*-PLL(N2IM-IM)] or dimethyl 3,3′-dithiobispropionimidate (DTBP) [yielding PEG-*b*-PLL(MPA)], with modifications aimed to impart disulfide cross-linking ability without compromising cationic charge. These two lysine modification reagents resulted in vastly different chemistry contained in the reacted block copolymer, which affected micelle formation behavior and stability along with in vitro and in vivo performance. Amidines formed with 2-IT were unstable and rearranged into a noncharged ring structure lacking free thiol functionality, whereas amidines generated with DTBP were stable. Micelles formed with siRNA and PEG-*b*-PLL(N2IM-IM) at higher molar ratios of polymer/siRNA, while PEG-*b*-PLL(MPA) produced micelles only near stoichiometric molar ratios. In vitro gene silencing was highest for PEG-*b*-PLL(MPA)/siRNA micelles, which were also more sensitive to disruption under disulfide-reducing conditions. Blood circulation was most improved for PEG-*b*-PLL(N2IM-IM)/siRNA micelles, with a circulation half-life 3× longer than naked siRNA. Both micelle formulations are promising for siRNA delivery applications in vitro and in vivo.

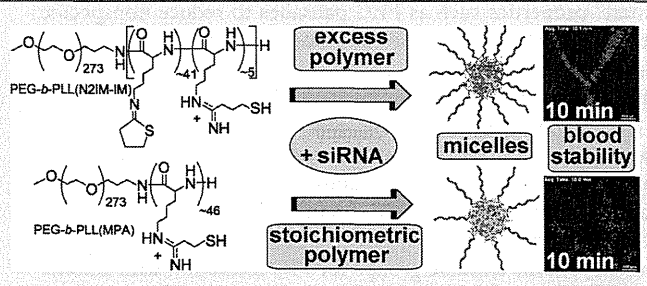

INTRODUCTION

Small interfering ribonucleic acid (siRNA) is capable of sequence-specific gene silencing without altering the host genome, a property that could be exploited to suppress proteins associated with disease. Thus, there is a strong impetus for development of practical, safe, and effective siRNA-based therapies. However, the inherent properties of siRNA molecules such as large size, anionic nature, and susceptibility to degradation preclude direct use for treatment of disease. Many clever materials have been developed that encapsulate siRNA until the intracellular site of activity is reached to improve its therapeutic activity. Structures formed after encapsulation of siRNA are often referred to as "siRNA carriers" or "siRNA delivery systems". To date, the types of materials explored as siRNA carriers include cationic lipids, cyclodextrins, branched and linear polycations, cationic block copolymers, and various peptides. General siRNA delivery strategies and considerations for the design of appropriate carriers have recently been reviewed.[1,2]

Polyion complexes (PICs) are often used to bind and encapsulate siRNA by exploiting its anionic nature.[3] PIC formation is a widely used strategy for preparation of advanced materials

Received: May 17, 2011
Revised: July 2, 2011
Published: August 24, 2011

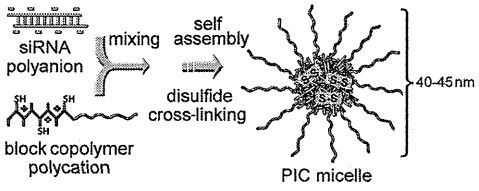

Figure 1. Preparation of disulfide cross-linked PIC micelles containing siRNA.

and diagnostics in the field of biomedical technology. PIC-based materials form by electrostatic attraction of oppositely charged polymers, with the release of water solvating charged functional groups providing further energetic gain. These functional materials may exploit single pairs of polyelectrolytes or multiple layering of charged polymers, with polyions from both natural and synthetic origin commonly used. The general strategy of PIC formation has been applied to prepare drug delivery systems, capture analytes for sensors, and form surface coatings, in addition to the formation of polyplexes with nucleic acids as described here.[4−7] PIC formation between nucleic acids and polycations generally results in nanosized structures with morphologies ranging from spheres to rods.[8] Furthermore, advanced PIC-based nucleic acid carriers have been engineered to contain "smart" properties such as PEG palisades to reduce nonspecific interactions with biological components, targeting ligands for tissue-specific accumulation, and also mechanisms for site-specific cargo release through environment-sensitive chemistries.[9−13]

Recently, we reported a PIC micelle siRNA delivery system prepared from the block copolymer poly(ethylene glycol)-*block*-poly(L-lysine) (PEG-*b*-PLL) modified with the cross-linking reagent 2-iminothiolane (2-IT, Traut's reagent).[14] The resulting block copolymer, termed PEG-*b*-PLL(IM), was designed to contain cationic amidine groups for PIC formation with anionic siRNAs and also free sulfhydryls to allow disulfide cross-linking in the micelle core for improved stability. Covalent disulfide cross-links are particularly attractive for micelle core stabilization because they are reversible and more susceptible to cleavage (reduction) at the subcellular site of activity where the levels of natural disulfide reducing agents are higher than in the bloodstream.[15] Disulfide cross-linked PIC micelle formation between siRNA and thiol-modified cationic block copolymer is shown in Figure 1.

Modification of PEG-*b*-PLL with 2-IT improved the quality of the resulting micelles (controlled size and PDI), increased micelle stability, and enhanced siRNA activity in vitro. However, micelles formed only at specific molar ratios of polymer/siRNA, and this optimal ratio increased with increased IM content in the PLL block. One possible explanation for this observed complexation behavior between PEG-*b*-PLL(IM) and siRNA could be related to the instability of amidines formed with 2-iminothiolane. Rearrangement of 2-IT modified amines is known to occur following reaction with amino acids and involves intramolecular reaction of sulfur with the amidine carbon, subsequent release of ammonia, and formation of a N-substituted 2-iminothiolane ring. This five-membered ring structure contains an imine bond ($pK_a \sim 6.7$) not an amidine ($pK_a \sim 12$), thus, reducing the positive charge of the block copolymer at pH 7.4.[16,17]

The focus of this work was to better understand the micelle formation behavior between PEG-*b*-PLL(IM) and siRNA, with the hypothesis that formation of N-substituted 2-iminothiolanes affects the formation and properties of micelles. This was accomplished by comparing 2-IT with the analogous amine-reactive amidination reagent, dimethyl 3,3′-dithiobispropionimidate (DTBP), to yield PEG-*b*-PLL(MPA). DTBP differs from 2-IT by a methylene unit between the thiol and amidine functional group, which prevents formation of N-substituted 2-iminothiolane ring structures due to the instability of a 4-membered ring. Comparison between the two polymer analogues clarified the siRNA complexation behavior previously observed for PEG-*b*-PLL(IM) and also provided insight into the structure−function relationship between the block copolymer component and the properties of resulting micelle structures. Micelle formulations prepared from both block copolymers represent improvements compared to naked siRNA and noncross-linked PICs, and are promising candidates for further development.

In this study we directly observed both N-substituted 2-iminothiolane rings and also linear 1-(4-mercaptobutyl) amidine groups upon ^{1}H NMR analysis of the reaction product of PEG-*b*-PLL with 2-IT, and have named the polymer "PEG-*b*-PLL-(N2IM-IM)".

EXPERIMENTAL SECTION

General. *N*-Methyl-2-pyrrolidinone (NMP, 99.5% anhydrous), LiCl (>99%), sodium tetraborate decahydrate (99.5%), diisopropylethylamine (DIPEA, 99.5%), 2N HCl solution, D_2O (99.9%), tetramethylsilane (TMS, 99.5%), and DCl (35% in D_2O) were obtained from Sigma Aldrich (St. Louis, MO) and used without further purification. 2-Iminothiolane hydrochloride (2-IT), diethyl ether (99+%), dithiothreitol (DTT, molecular biology grade DNase and RNase free), ethylenediamine tetraacetic acid disodium salt dihydrate (EDTA, 99.5%), sodium bicarbonate (99.5−100.3%), sodium dihydrogen phosphate·$2H_2O$ (99−102%), disodium hydrogen phosphate·$12H_2O$ (99+%), glutathione (reduced form), and sodium chloride (99+%) were supplied by Wako Pure Chemical Industries (Osaka, Japan). Dimethyl 3,3′-dithiobispropionimidate·2HCl (DTBP), Ellman's reagent [5,5-dithiobis-(2-nitrobenzoic acid)], 2,4,6-trinitrobenzene sulfonic acid (5% w/v in methanol), and slide-a-lyzer dialysis cassettes (MWCO = 3.5 kDa) were obtained from Thermo Scientific (Rockford IL). Sterile HEPES (1 M, pH 7.3) was purchased from Amresco (Solon, OH). Spectra/Por dialysis tubing (10 KDa MWCO) was acquired from Spectrum Laboratories (Rancho Dominguez, CA). Firefly GL3 luciferase siRNA (sense: 5′-CUU ACG CUG AGU ACU UCG AdTdT-3′; antisense: 5′-UCG AAG UAC UCA GCG UAA GdTdT-3′) Cy3-labeled firefly luciferase siRNA, Cy5-labeled firefly luciferase siRNA, and scramble siRNA (sense: 5′-UUC UCC GAA CGU GUC ACG UdTdT-3′; antisense: 5′-ACG UGA CAG GUU CGG AGA AdTdT-3′) were synthesized by Hokkaido System Science Co., Ltd. (Hokkaido, Japan) with dye labels attached to the sense strands.

^{1}H NMR analysis of PEG-*b*-PLL(N2IM-IM) was conducted in D_2O containing 0.05% v/v tetramethylsilane and 3 μL/mL DCl solution (35% DCl in D_2O) at 22 °C using a 300 MHz spectrometer (EX 300, JEOL, Tokyo, Japan). ^{1}H NMR analysis of PEG-*b*-PLL(MPA) and PEG-*b*-PLL was conducted in the same fashion as PEG-*b*-PLL(N2IM-IM) except without DCl.

Static and dynamic light scattering measurements were performed at 25 °C on a ZetaSizer Nano ZS instrument (Malvern Instruments Ltd., Malvern, U.K.) equipped with a He−Ne laser (λ = 633 nm) as the incident beam with samples (16 μL) loaded into a Zen 2112 low-volume cuvette. Absorbance and fluorescence measurements were performed with NanoDrop ND-1000 and ND-3300 instruments (NanoDrop Technologies Inc., Rockland DE), respectively.

Scheme 1. Synthesis of PEG-*b*-PLL Derivatives

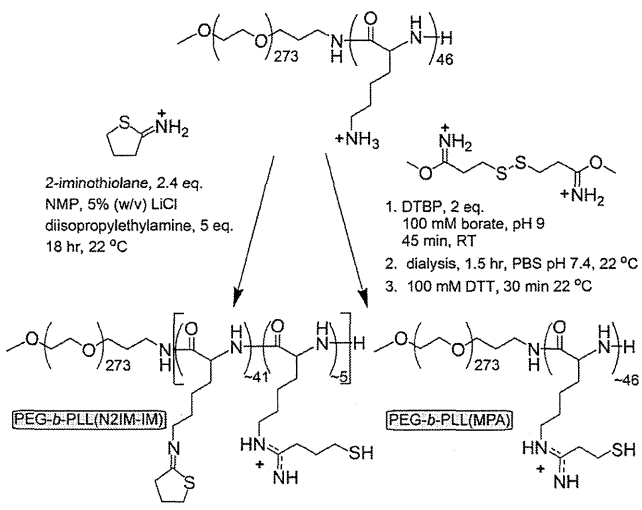

The luciferase-expressing mouse melanoma cancer cell line, B16F10-luc, was purchased from Caliper LifeScience (Hopkinton, MA). Dulbecco's modified eagle's medium (DMEM) was obtained from Sigma Aldrich (St. Louis, MO). Fetal bovine serum was provided by Dainippon Sumitomo Pharma Co. (Osaka, Japan). Falcon Easy-Grip 35 × 10 mm vacuum gas plasma-treated polystyrene tissue culture dishes were obtained from BD Biosciences (San Jose, CA). Luciferin was purchased from Summit Pharmaceutical International (Tokyo, Japan). Luciferase bioluminescence in B16F10-luc cells was measured using an ATTO Kronos Dio photon countable incubator (ATTO Corp., Tokyo, Japan).

Synthesis of PEG-*b*-PLL(N2IM-IM). PEG-*b*-PLL copolymer was synthesized as previously described, comprising a 12000 MW PEG segment and a 45 amino acid PLL segment.[13,18] Iminothiolane modification of PEG-*b*-PLL was achieved by reacting primary amino groups contained in the side chains of PLL with 2-IT, as outlined in Scheme 1. First, 50 mg PEG-*b*-PLL (0.12 mmol amine, 1 equiv) was added to 2 mL NMP containing 5 wt % LiCl and the reaction vessel was purged with Ar and then capped with a septum. The polymer solution was placed into an oil bath at 50 °C and stirred for 30 min to completely dissolve all solids. After dissolution of polymer, the solution was removed from heat and cooled to 22 °C. Next, DIPEA (100 μL, 1.1 mmol, 5 equiv relative to Lys amines) was added to the polymer solution under Ar through the septum. Finally, 2-iminothiolane·HCl (39 mg, 0.28 mmol, 2.4 equiv relative to lysine amines) was added directly to the polymer solution. The reaction continued with stirring for 18 h at 22 °C under an argon atmosphere. After 18 h, the reaction was terminated by precipitation into a 10× volume excess of dry diethyl ether. Precipitated product was washed several times with ether and dried under vacuum to a constant mass. Crude product was redissolved in PBS buffer (10 mM phosphate, 150 mM NaCl, pH 6.0) and then dialyzed (SpectraPor7, 10 kDa MWCO) against PBS pH 6.0 for one day and distilled water for one day with frequent media changes. Dialyzed polymer solution was passed through a 0.2 μM filter and then lyophilized. Yield: 55 mg (96%), white powder. The degree of lysine modification was determined from the ^{1}H NMR spectra recorded in acidic D_2O (Figure 2) by the peak intensity ratio of the β, γ, and δ-methylene protons of Lys ($(CH_2)_3$, δ = 1.3–1.9 ppm) to the sum of peak intensities of methylene protons from the C4 carbon of N-substituted 2-iminothiolane groups and the protons of trimethylene units of mercaptopropyl groups (HS-$(CH_2)_3$, δ = 2.1, 2.6, and 2.8 ppm). The calculated IM introduction rate was 95%. The ratio of 1-(4-mercaptobutyl) amidine groups to N-substituted 2-iminothiolane groups was determined by the peak intensity ratios of methylene protons from the C4 position on N-substituted 2-iminothiolane groups (2.4 ppm) and protons of trimethylene units of mercaptopropyl groups (HS-$(CH_2)_3$, δ = 2.1, 2.6, and 2.8 ppm). The ratio of 1-(4-mercaptobutyl) amidine to N-substituted 2-iminothiolane was ~0.25.

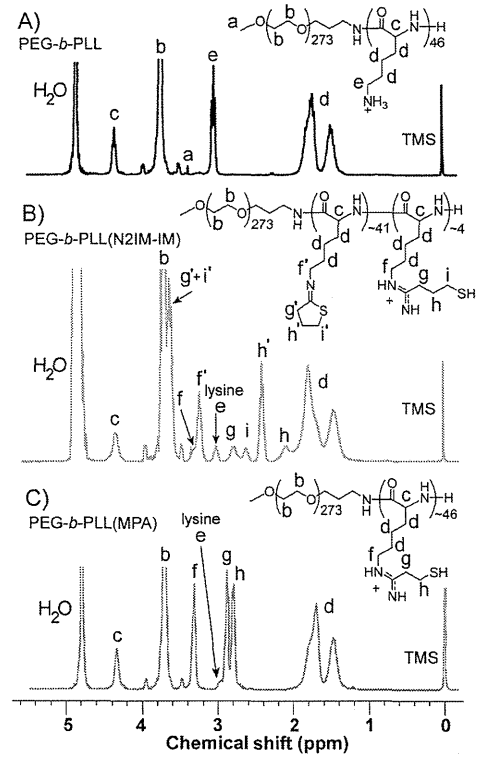

Figure 2. ^{1}H NMR spectra of PEG-*b*-PLL and modification products. Spectra were recorded at 300 mHz, 25 °C in D_2O (A,C) or D_2O containing 3 μL/mL 35% DCl solution (B). Residual lysine residues are not included in the chemical structures shown in (B) and (C).

Synthesis of PEG-*b*-PLL(MPA). PEG-*b*-PLL(MPA) was synthesized by reaction of lysine primary amines with amido esters contained in DTBP as shown in Scheme 1. First, PEG-*b*-PLL (300 mg, 0.7 mmol amines, 1 equiv) of the same parent stock used for synthesis of PEG-*b*-PLL(N2IM-IM) was dissolved in 100 mM sodium borate, pH 9.0 (60 mL) and then DTBP·HCl (439 mg, 1.4 mmol, 2 equiv relative to lysine amines) was added to the polymer solution. The reaction was stirred at room temperature for 45 min and then transferred to slide-a-lyzer dialysis cassettes (MWCO 3500) and dialyzed against PBS (10 mM phosphate, 150 mM NaCl, pH 7.4) for 1.5 h to remove unreacted DTBP. The reaction mixture was recovered and then DTT (300 mg) was added to generate the free sulfhydryl in polymer-reacted DTBP. The reaction was stirred at room temperature for 30 min and then transferred to slide-a-lyzer dialysis cassettes (MWCO 3500). Dialysis was performed against 10 mM PBS, pH 6.0 for 2 h and then distilled water for 2 h with rapid stirring and frequent exchange of dialysis media. The purified polymer solution was passed through a 0.2 μm filter and lyophilized. Yield: 299 mg (73%), white powder. The degree of DTBP introduction was determined from the ^{1}H NMR spectra shown in Figure 2 by the peak intensity ratio of the β, γ, and δ-methylene protons of Lys ($(CH_2)_3$, δ = 1.3–1.9 ppm) to the protons of mercaptoethyl groups (HS-$(CH_2)_2$, δ = 2.7–2.9 ppm). The calculated degree of lysine modification was 95%.

Analysis of Thiol Content in Block Copolymers. Free thiol content in modified block copolymers was determined by Ellman's assay.[19] Polymer solutions (5 mg/mL) were incubated in 10 mM HEPES buffer containing 5 mM EDTA and 15 mM DTT for 30 min

Table 1. Summary of Polymer and Micelle Properties

	PEG-*b*-PLL[l]	PEG-*b*-PLL(N2IM-IM)	PEG-*b*-PLL(MPA)
MW[a]	19600	22000	23350
% modified lysines[b]	0	95	95
% thiol content[c]	0.7 ± 0.04	11 ± 2.5	90 ± 12
polymer/siRNA molar ratio with maximum SLI at pH 7.4/5.0[d]	1.2/ND	≥7.6/1.4	1.2/1.3
micelle size (d.nm)[e,f,g]	194 ± 15	42.4 ± 2.2	41.8 ± 2.1
micelle PDI[e,g]	0.44 ± 0.1	0.07 ± 0.02	0.05 ± 0.02
micelle ζ potential[g]	ND	−1.99 ± 0.47	−0.50 ± 1.26
micelle stability in 600 mM NaCl[d,g,h]	<5%	86%	43%
% remaining thiol in cross-linked micelles[c,i]	ND	52 ± 0.54	3.7 ± 0.27
maximum gene silencing[g,j]	<5%	~12%	~40%
circulation half-life[g,k]	~ 3 min	~10 min	~6 min

[a] Including chloride counterion. [b] Determined by ^{1}H NMR. [c] Determined by Ellman's Assay. [d] Determined by static light scattering, 25 °C. [e] Determined by dynamic light scattering, pH 7.4, 25 °C. [f] Reported as the *z*-average cumulant mean diameter. [g] Cross-linked micelles prepared at the polymer/siRNA molar ratio of max SLI. [h] Stability relative to cross-linked micelles in 10 mM HEPES, pH 7.4. [i] Expressed relative to the free thiol content measured in polymer before micelle formation. [j] Determined in B16F10-luc cancer cells, 200 nM siRNA, 48 h. [k] Determined by in vivo confocal intravital microvideography, 24 μg siRNA injection. [l] Structures formed with siRNA may not be micelles due to their large size and PDI.

at room temperature to reduce any disulfides present. The reduced polymer solution was placed on ice and handled in a timely manner at 0−4 °C until the addition of Ellman's reagent. After reduction, DTT was removed from the polymer solution using a NanoSep centrifugation device (3000 MWCO). Samples were subjected to three successive concentration/rinsing cycles with 10 mM HEPES containing 5 mM EDTA as the rinsing buffer. After the final centrifugation cycle, concentrated polymer solution was collected and diluted to its original volume. The final flow-through fraction was also collected and diluted in the same manner as the polymer-containing fraction to determine the amount of DTT remaining in the sample. Polymer and flow through samples were subjected to Ellman's assay according to the manufacturers protocol and sample absorbance was measured at 412 nm. Free thiol content of solutions was determined from a standard curve generated with reduced glutathione, and the thiol content in the polymer fraction was obtained by subtracting the thiol content in the flow-through fraction to correct for residual DTT. PEG-*b*-PLL was analyzed as a negative control in a similar fashion, except the polymer solution (5 mg/mL) was used directly without DTT incubation.

Complexation of Block Copolymers with siRNA. Block copolymer complexation and micelle formation with siRNA was studied as a function of the molar ratio of polymer/siRNA using the polymer molecular weights shown in Table 1. It should be noted that siRNA contains 40 negative charges and the poly(L-lysine) segment in the block copolymer contains ~46 units. Thus, if all modified PLL side-chains are charged the polymer/siRNA molar ratio and +/− charge ratio are nearly interchangeable. Polymer samples were dissolved in 10 mM HEPES buffer (pH 7.4) at a concentration of 5 mg/mL and aliquots were further diluted from this stock solution for preparation of complexation mixtures with siRNA. PEG-*b*-PLL(MPA) polymer solutions were diluted first with HEPES buffer to generate a solution twice the concentration desired for mixing with siRNA, and then 1:1 with HEPES buffer containing 30.54 mg/mL DTT. PEG-*b*-PLL(N2IM-IM) polymer solutions were reduced by direct addition of DTT to the 5 mg/mL polymer stock solution to yield 15.25 mg/mL DTT. Polymer solutions were incubated for 30 min at room temperature after addition of DTT to ensure cleavage of any disulfides present. Complexation was achieved by mixing polymer solution with siRNA (15 μM in 10 mM HEPES buffer, pH 7.4) at a volume ratio of 1:2 (polymer/siRNA) and PIC micelles were allowed to form for 24 h at 25 °C. For micelle formation at pH 5.0, both reduced polymer and siRNA solutions were acidified with appropriate volumes of 0.05 M HCl prior to mixing, then combined immediately. Disulfide cross-linked micelles were prepared by dialysis (slide-a-lyzer cassette (MWCO 3.5 kDa)) against 10 mM HEPES pH 7.4 containing 0.5% v/v DMSO for 2 days, followed by 2 days of dialysis against HEPES for removal of DMSO. DMSO was included in the dialysis buffer to assist in disulfide formation, as it is a mild oxidant specific toward thiols.[20] All disulfide cross-linked micelle samples were prepared at the polymer/siRNA molar ratio that exhibited maximum light scattering intensity in optimization experiments, polymer/siRNA = 7.6 for PEG-*b*-PLL(N2IM-IM) and 1.3 for PEG-*b*-PLL(MPA). Free thiol content in cross-linked micelles was determined using the Elman's assay according to the manufacturers protocol by sample absorbance at 412 nm and a standard curve generated with reduced glutathione. PEG-*b*-PLL(N2IM-IM) micelles were used directly for the assay whereas PEG-*b*-PLL(MPA)/siRNA micelles were concentrated 4-fold using NanoSep centrifugation devices (3000 MWCO) to yield a micelle solution with a theoretical thiol content within the range of the calibration curve.

Characterization of Micelles. PIC micelle solutions were analyzed by static and dynamic light scattering (DLS) to determine scattered light intensity (SLI) and PIC micelle size/PDI, respectively. Size distributions were determined by cumulant and histogram analysis of DLS data. Results are shown as the *z*-average diameter (cumulant mean) with the polydispersity index (PDI) (defined in the ISO standard document 13321:1996) and histogram of size distribution, as determined by the software provided by the manufacturer. The ζ-potentials of cross-linked PIC micelles prepared at the polymer/siRNA molar ratio with maximum SLI were measured in 10 mM HEPES buffer (pH 7.4) containing 150 mM NaCl at 37 °C. All samples were equilibrated to the defined temperature for 2 h prior to measurement. For fluorescence quenching experiments, PIC micelle solutions were prepared at various polymer/siRNA molar ratios as described above except Cy3-labeled GL3 siRNA was used. After 24 h incubation in the dark at 25 °C, the fluorescence intensity was measured with a NanoDrop ND-3300 instrument using white LED excitation.

In Vitro Stability of Micelles. Disulfide cross-linked PIC micelle stability was measured as a function of NaCl concentration in the presence or absence of the disulfide reducing agent DTT. Cross-linked micelle samples were diluted 1:1 with NaCl solution at desired concentrations and incubated at 37 °C for 24 h. Samples subjected to disulfide reducing conditions were diluted in the same fashion as above, however, with NaCl solutions containing 200 mM DTT. After the 24 h incubation period, samples were measured by static and dynamic light scattering, as described in the micelle characterization section.

TEM Analysis of Cross-Linked Micelles. Cross-linked micelle morphology was directly observed by transmission electron microscopy (TEM). For each analysis, the nucleic acid stain uranyl acetate (10 μL of a 2% w/v solution) was deposited onto a glass slide followed by sample solution (10 μL). This mixture was allowed to stand for 30 s in order to achieve effective staining. A carbon-coated 400 mesh Cu grid (Nisshin EM) was then immersed into the sample, allowing both sides of the grid to become fairly saturated. The grid was air-dried on a piece of filter paper and then transferred to a H-7000 TEM (Hitachi Ltd., Tokyo, Japan) for imaging. Images were recorded at optical magnifications of 50000 and 80000 with an acceleration voltage of 75 kV.

Micelle size distributions were determined from TEM images using ImageJ (available online at http://rsb.info.nih.gov/ij/download.html). TEM images previously modified by the addition of a scale bar were uploaded onto a computer and opened with ImageJ. A pixel to nanometer conversion value was generated by manually drawing a line on the scale bar and utilizing the program's built in Analyze → Set Scale command. Following creation of the pixel:nanometer conversion factor, lines were drawn by hand on each individual particle and their nanometer value was obtained via the Analyze → Measure command. A total of 46 particles were analyzed from each image. The raw data was imported into Microsoft Excel and histograms were generated.

In Vitro Gene Silencing. The gene silencing activity of siRNA incorporated in cross-linked micelles was determined in B16F10 murine melanoma cancer cells stably expressing luciferase (B16F10-luc), with luciferase targeted for gene knockdown. Cross-linked micelles containing GL3 (target) or scramble (off-target) siRNA were prepared as described above. Cells were cultured in Dulbecco's modified eagle's medium (DMEM) containing 10% fetal bovine serum (FBS). B16F10-luc cells were seeded onto 35 mm Petri dishes (25000 cells/dish) and allowed to attach for 24 h. After cell attachment, the media was removed and replaced with media (2 mL) containing 100 μM luciferin and cross-linked micelles corresponding to 200 nM micelle-encapsulated siRNA. For each analysis, control cell samples were prepared by addition of media diluted with HEPES instead of micelle solution. The total dilution of media after addition of luciferin and micelle solution was less than 200 μL additives per 10 mL of media. Samples were placed into a Kronos real-time photon-countable incubator and the luminescence intensity was measured periodically over a 55 h time period, with the temperature and CO_2 maintained at 37 °C and 5%. The amount of gene silencing was determined by dividing the average luminescence intensity of treated samples by the average luminescence intensity of control samples, $n = 4$.

In Vivo Micelle Stability. SiRNA incorporating micelle stability in the blood compartment was evaluated using intravital confocal videography in live mice. All picture/movie acquisitions were performed using a Nikon A1R confocal laser scanning microscope system attached to an upright ECLIPSE FN1 (Nikon Corp., Tokyo, Japan) equipped with a 20× objective, 640 nm diode laser, and a band-pass emission filter of 700/75 nm. The pinhole diameter was set to result in a 10 μm optical slice. Eight-week-old female BALB/c nude mice (Oriental Yeast Co., Ltd., Tokyo, Japan) were anesthetized with 2.0−3.0% isoflurane (Abbott Japan Co., Ltd., Tokyo, Japan) using a Univenter 400 Anaesthesia Unit (Univentor Ltd., Zejtun, Malta). Mice were then subjected to lateral tail vein catheterization with a 30-gauge needle (Becton, Dickinson and Co, Franklin Lakes, NJ, U.S.A.) connected to a nontoxic medical grade polyethylene tube (Natsume Seisakusho Co., Ltd., Tokyo, Japan). Anesthetized mice were placed onto a temperature-controlled pad (Thermoplate; Tokai Hit Co., Ltd., Shizuoka, Japan) integrated into the microscope stage and maintained in a sedated state throughout the measurement. Ear lobe dermis was observed without surgery and was easily fixed beneath a coverslip with a single drop of immersion oil. Data was acquired in video mode for 3 min (30 frames/sec), followed by snapshots every 1 min thereafter. All animal experimental procedures were performed in accordance with the Guide for the Care and Use of Laboratory Animals as stated by the National Institutes of Health.

Micelles prepared with Cy5-labeled siRNA at the polymer/siRNA molar ratio corresponding to maximum SLI (7.6 for PEG-*b*-PLL(N2IM-IM) and 1.2 for PEG-*b*-PLL(MPA)) were injected (200 μL of 9.2 μM siRNA, ~24 μg total siRNA) via the tail vein 10 s after the start of video capture. Micelles prepared with PEG-*b*-PLL(N2IM-IM) or PEG-*b*-PLL(MPA) and siRNA were cross-linked, as described above before injection.

Video data was analyzed by selecting regions of interest (ROIs) within blood vessels or extravascular skin tissue and the average fluorescence intensity per pixel for each time point was determined using the Nikon NIS-Elements C software provided by the manufacturer. To produce the blood retention profiles shown in Figure 6, vein fluorescence data was expressed relative to the maximum observed value. First, the background fluorescence intensity was determined from video captured during the 10 s before sample injection. This background value was then subtracted from the average pixel intensities measured after micelle injection to create background-corrected intensities for each time point. Next, relative fluorescence intensities were determined by dividing the average fluorescence intensity at each time point by the maximum observed fluorescence intensity (typically observed ~1 min). Analysis of tissue fluorescence intensity was performed in the same manner, without normalizing to the maximum observed value. Each experiment was performed in duplicate in separate animals, with representative data from a single animal shown in Figure 6. Individual circulation data for each mouse is provided as Supporting Information. A detailed description of the microscope apparatus and mouse positioning for intravital confocal micro videography, as well as examples of data workup showing ROIs can be found in our previously published report.[21]

RESULTS

Modification of PEG-*b*-PLL with 2-IT. PEG-*b*-PLL was reacted with excess 2-IT under organic conditions, as previously described, except 2-IT was added directly to the reaction mixture as a solid instead of dropwise addition of a solution.[14] The reaction proceeded by nucleophilic attack of lysine amine groups on the imine carbon contained in 2-IT, followed by ring-opening and generation of the free sulfhydryl (which may subsequently react with the amidine carbon as discussed below). Analysis of the PEG-*b*-PLL(N2IM-IM) polymer product by ^{1}H NMR spectroscopy showed that the desired modification was successful, as the lysine ε-CH_2 peak was shifted downfield and methylene peaks corresponding to N2IM and IM groups appeared in the spectrum (Figure 2). Both linear 1-(4-mercaptobutyl) amidine and cyclic N-substituted 2-iminothiolane groups were observed in the product, with the majority of side chains (~75%) being in the closed ring form based on integration values. Nearly complete conversion (95%) of lysine amine groups was achieved by this synthesis procedure. It should be noted that 2 mol equiv of 2-IT (relative to lysine amines) is necessary to achieve nearly complete modification of lysine amines. Addition of 1 mol equiv of 2-IT resulted in only ~60% conversion of lysine amines (data not shown).

2-IT modified polymer product was soluble in buffer despite the loss of charged functional groups. However, polymer self-association at 10 mg/mL interfered with ^{1}H NMR analysis in D_2O and acidification of the sample greatly clarified the spectrum. PEG-*b*-PLL(N2IM-IM) polymer solution showed very little light scattering at the concentration used for siRNA complexation (1.67 mg/mL) and addition of siRNA to the polymer

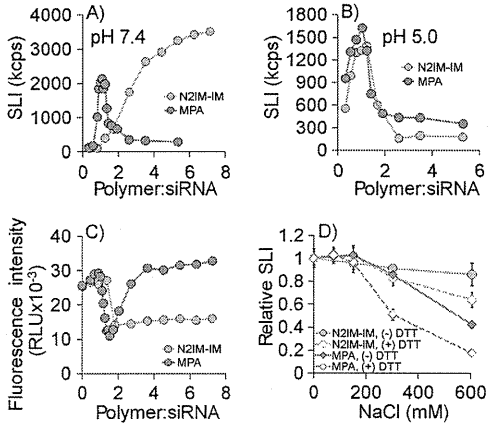

Figure 3. Light scattering behavior of siRNA and PEG-*b*-PLL(X) (*X* = N2IM-IM or MPA) mixtures, fluorescence quenching, and the stability of resulting cross-linked micelles. (A) Complexation of block copolymers with siRNA at pH 7.4, 25 °C. (B) Complexation of block copolymers with siRNA at pH 5.0, 25 °C. (C) Fluorescence quenching of Cy3-siRNA/block copolymer mixtures at pH 7.4, 25 °C. (D) Stability of disulfide cross-linked micelles following 24 h incubation at 37 °C in NaCl solutions with or without disulfide reducing agent (DTT). Data represents the average value ± standard deviation, $n = 3$. All polymer/siRNA ratios are molar ratios.

solution resulted in a 10-fold increase in scattered light intensity. A detailed analysis of polymer solution light scattering at pH 7.4 and 4.0 is available as Supporting Information.

Modification of PEG-*b*-PLL with DTBP. PEG-*b*-PLL was modified with DTBP under aqueous conditions. Nucleophilic reaction of lysine primary amine groups with imidoester groups contained in DTBP resulted in formation of the amidine with concurrent release of methanol. The reaction pH of 9.0 was chosen to minimize side reactions that are described to occur with imidoesters below pH 8.0.[22] A molar excess amount of DTBP was used to minimize polymer cross-linking, which is expected to occur due to the bifunctional nature of this reagent. A total of 2 molar equiv of DTBP relative to lysine amines used in the polymer modification reaction corresponded to 4 equiv of reactive amido esters. Unreacted DTBP was removed from the reaction mixture prior to disulfide cleavage of polymer-reacted DTBP to allow more efficient reduction with DTT. Reaction of the DTBP-modified polymer with DTT resulted in cleavage of the internal disulfide and generation of the desired 1-(3-mercaptopropyl) amidine functionality. DTT was removed quickly and efficiently (~4 h) using high surface area slide-a-lyzer dialysis cassettes, as DTT was not detected in the ^{1}H NMR spectrum of the obtained product (Figure 2). Successful modification of lysine amines with DTBP was confirmed by ^{1}H NMR spectroscopy, as indicated by the downfield shift of lysine ε-CH_2 groups and the appearance of two methylene peaks corresponding to those found in DTBP (Figure 2). The degree of lysine modification was 95% under the reaction conditions used in this study.

Analysis of Thiol Content in Modified PEG-*b*-PLLs. Free thiol content in PEG-*b*-PLL(N2IM-IM) and PEG-*b*-PLL(MPA) was determined using Ellman's assay, which is based on reaction of 5,5-dithio-bis-(2-nitrobenzoic acid) with sulfhydryls at basic pH to generate a colored thiolate derivative. The measured thiol content was quite different between PEG-*b*-PLL(N2IM-IM) and PEG-*b*-PLL(MPA), as shown in Table 1. PEG-*b*-PLL(MPA) thiol content was near the theoretical value assuming complete reaction of lysine amines (90 ± 10%), whereas PEG-*b*-PLL(N2IM-IM) thiol content was much lower (11 ± 2%). The low amount of free sulfhydryl detected in PEG-*b*-PLL(N2IM-IM) is consistent with the formation of N-substituted 2-iminothiolanes, which lack free thiol functionality.

Preparation and Characterization of PIC Micelles Formed with siRNA. PIC micelles formed spontaneously upon mixing polymer and siRNA solutions under reducing conditions, as evidenced by increased scattered light intensity and the presence of particles less than 100 nm in size with low PDI (<0.1, i.e., spherical). At pH 7.4, PIC micelles formed at higher polymer/siRNA molar ratios for PEG-*b*-PLL(N2IM-IM) (polymer/siRNA = 3.6–7.6) and only at near stoichiometric ratios for PEG-*b*-PLL(MPA) (polymer/siRNA = 1.0–1.3, Figure 3A). Addition of excess polymer in the case of PEG-*b*-PLL(MPA) resulted in a sharp decrease in SLI, showing that excess polycation disrupts micelle formation. DLS analysis of micelle solutions revealed the formation of narrowly dispersed (PDI <0.1) particles 40–45 nm in size at the optimal polymer/siRNA mixing ratio for both block copolymers, which is consistent with values expected for spherical micelle structures (Table 1). Detailed light scattering data for complexation solutions (non-cross-linked) at each polymer/siRNA molar ratio is available as Supporting Information. Analysis of the ζ-potential of cross-linked micelle structures formed at the optimal polymer/siRNA molar ratio indicated a near-neutral value for both PEG-*b*-PLL(N2IM-IM) and PEG-*b*-PLL(MPA), which is expected for core–shell micelle structures where the core charge is shielded by the PEG corona (Table 1). Essentially no free-thiol was detected in cross-linked micelles prepared with PEG-*b*-PLL(MPA), but ~50% free thiol (relative to the original 11% thiol-containing PLL side chains measured in polymer only) was observed in micelles prepared with PEG-*b*-PLL(N2IM-IM) when subjected to Ellman's assay (Table 1). This result shows that both free thiol content and disulfide cross-linking efficiency was reduced in PEG-*b*-PLL(N2IM-IM).

Complexation behavior between PEG-*b*-PLL(N2IM-IM) and siRNA changed under acidic conditions, whereas PEG-*b*-PLL(MPA) complexation behavior with siRNA did not (Figure 3B). For PEG-*b*-PLL(N2IM-IM), the polymer/siRNA molar ratios corresponding to the maximum SLI value shifted from ~7.6 to lower values near the stoichiometric region. This observation confirmed that protonation of imines present in N-substituted 2-iminothiolane structures can restore the cationic nature of PEG-*b*-PLL(N2IM-IM). On the other hand, PEG-*b*-PLL(MPA) micelle formation behavior was unaffected by lowering the pH of complexation conditions and the polymer/siRNA molar ratio for maximum SLI remained in the stoichiometric region at both pH 7.4 and 5.0. Micelle size and PDI at the polymer/siRNA molar ratio corresponding to maximum SLI did not change for either polymer upon complexation at lower pH (data not shown).

Fluorescence Quenching Studies. PEG-*b*-PLL(N2IM-IM) and PEG-*b*-PLL(MPA) complexation with siRNA was also investigated by monitoring the fluorescence quenching of Cy3-labeled siRNA (Figure 3C). Fluorescence quenching is expected to occur only upon formation of micelle structures through dye–dye interactions or interaction with amines contained in the micelle core.[23–25] Cy3 fluorescence was quenched considerably upon formation of micelles between both block copolymers and siRNA. For PEG-*b*-PLL(MPA), maximum fluorescence quenching was concurrent with the polymer/siRNA molar ratio that resulted in the maximum SLI observed in light scattering